Chemical Properties of Alkenes and Alkynes from Carbon 1s Photoelectron Spectroscopy and Theory

Alf Holme

Thesis for the Degree of Philosophiae Doctor (PhD)
Department of Chemistry
University of Bergen, Norway
December 2012

To Mari, Vibeke, family and friends.

"The molecule also has a body. When this body is hit, the molecule feels hurt all over."
– A. Kitaigorodski.

Acknowledgments

There are many people who in one way or another have contributed to my thesis. First of all, I would like to thank my two supervisors, Prof. Leif J. Sæthre and Prof. Knut J. Børve. Both of you have been fabulous, and I am deeply grateful for all the guidance, support and educational moments. Your expertise, enthusiasm and passion for electron spectroscopy have been a huge inspiration for me.

I spent four weeks at the Chemistry Department at Oregon State University in Corvallis, USA. I would like to thank Prof. T. D. Thomas for providing me an office place and making the stay possible. I thank you for all help and fruitful discussions. I would also like to thank Barbara and Tove for all support during my stay in Corvallis. Many thanks go to the staff at the Department, in particular Prof. Kenneth Hedberg and Prof. Joseph Nibler, for making the stay so nice.

I would like to thank Prof. Tom X. Carroll for all the discussions and Igor lessons. I also thank the MAX-lab staff, in particular Maxim Tchaplyguine at beamline I411, for all assistance and help during our experiments. Many thanks to Prof. Svante Svensson and co-workers from Uppsala and Lund University for all the moments at MAX-lab, conferences, and workshops. It has been a nice experience collaborating with you.

There are many people at the Department of Chemistry in Bergen who have contributed making the PhD period a joyful experience. I would like to thank the staff and colleagues, in particular Elaine, Maria, Jarle, Mathias, Mahmoud, Velaug, Nils, Randi, Annette, Sara, Christian, André, Bjarte, Ørjan, Wouter, Magnus, Yuri, Hjørdis, Dagfinn, Giovanni and Fredrik.

I also wish to thank my family and friends for all support, and I want to thank Eldbjørg for all the hours of babysitting! My very special thanks go to my dear Vibeke. Your unfailing love, support and encouragement have been of enormous importance to me! Finally, I wish to thank my sunshine Mari for all that you have given me!

Bergen, December 2012
Alf Holme

Abstract

The field of electron spectroscopy has evolved extensively the last couple of decades. On one hand, the technology at the synchrotron radiation facilities and of electron analyzers has improved, providing experimental data with more information about the sample. On the other, new and powerful computational resources have made it possible to analyze and increase our understanding of the experimental data. With these tools at hand, we are now in position to study molecular properties such as electronegativity, acidity, reactivity, and conformational isomerism.

X-ray photoelectron spectroscopy (XPS) is the preferred technique to explore inner-shell ionization energies. In the present work, carbon 1s photoelectron spectra of a series of alkenes and alkynes have been measured and analyzed. As the molecular size of the alkene or alkyne increases, the complexity of the spectrum increases correspondingly. In the most difficult cases, results from the spectral analyses often are neither credible nor reproducible. One way to avoid this situation, is to calculate shifts in carbon 1s ionization energy with high accuracy and use them as constraints in the spectral analysis. In this thesis, shifts have been calculated using a number of *ab initio* and density functional theory (DFT) methods. To get an overview of the most promising methods, theoretical shifts were compared with the corresponding experimental values.

Some of the larger systems in this thesis may possess two or more geometries obtained by rotation about carbon–carbon bonds. Such stable geometries are called conformers, and are an important and fundamental property of molecules. In the present work, XPS analyses are performed on a subset of alkenes and alkynes with the ability of possessing two or more conformers. It is shown that some of the conformers give rise to unique carbon 1s photoelectron spectra, and these are identified and used to determine the relative amount and stability of the different conformers.

Carbon 1s ionization energies of hydrocarbons depend on the ability of a carbon atom to accept a positive charge, and there are other chemical properties that also depend on this ability. This work investigates the relationship between carbon 1s ionization energies and chemical reactivity in electrophilic addition reactions for twelve pairs of alkenes and alkynes. The relative chemical reactivity of carbon-carbon double and triple bonds in pro-

ton addition reactions has been a recurrent question for decades, and this thesis facilitates a direct comparison of the reactivity of the two classes of compounds as seen from C1s spectroscopy as well as activation energies and enthalpies of protonation.

Contents

List of papers

This thesis is based on the following list of papers.

I Accuracy of calculated chemical shifts in carbon 1s ionization energies from single-reference *ab initio* methods and density-functional theory.
A. Holme, K. J. Børve, L. J. Sæthre and T. D. Thomas.
J. Chem. Theory Comput. **7**, 4104–4114 (2011).

II Carbon 1s photoelectron spectroscopy of 1-pentyne conformers.
A. Holme, L. J. Sæthre, K. J. Børve and T. D. Thomas.
J. Mol. Struct. **920**, 387–392 (2009).

III Conformations and CH/π interactions in aliphatic alkynes and alkenes.
A. Holme, K. J. Børve, L. J. Sæthre and T. D. Thomas.
Submitted.

IV Chemical reactivity of alkenes and alkynes as seen from activation energies, enthalpies of protonation, and carbon 1s ionization energies.
A. Holme, L. J. Sæthre, K. J. Børve and T. D. Thomas.
J. Org. Chem. **77**, 10105–10117 (2012).

Comments on my own participation

In this section, I comment on my own participation on the different papers this work is based on.

In paper I, I have contributed to the experimental work for only a few of the molecules that are included in the database. In this work, I took part in building the database, selecting molecules, performing the *ab initio* and DFT calculations, as well as the discussion of the results.

In paper II, I participated on the data acquisition of 1-pentyne, performed the analysis of the spectrum and a large share of the calculations, and participated on the writing of the first draft of the paper.

In paper III, I took part in the experimental measurements of many of the molecules included in the study. I performed most of the spectral analyses and computations, and participated in the writing of the first draft of the paper as well as finalizing the manuscript.

In paper IV, I have contributed to the experimental work for many of the molecules, and performed the spectral analyses and calculations for a larger fraction of the molecules included in the study. I participated on the writing of the first draft and the discussion and finalizing of the paper.

Chapter 1

Introduction

1.1 Photoelectron spectroscopy

Light, or electromagnetic radiation, makes the world visible to the human eye, and the colors of objects are dependent on their transmission, surface, and emission properties. There are several different processes that may lead to emission of light. One example is luminescence, where a substance emits light without heating it. Here, electrons are excited from one discrete energy level to a higher by absorbing radiation. This is followed by a deexcitation of the electrons, and radiation or *photons* are emitted. The photon energy (E) is directly proportional to the frequency (ν) and inversely proportional to the wavelength (λ) of the radiation, expressed in equation 1.1.

$$E = h\nu = \frac{hc}{\lambda} = E_B + E_K \tag{1.1}$$

Here, h is Planck's constant and c is the speed of light. When the photon energy exceeds the energy required to excite an electron to the highest possible state, the electron is left in an unbound state with an excess kinetic energy (E_K). This electron is called the photoelectron, and the energy required to remove the electron from the atom or molecule is referred to as the ionization energy or binding energy (E_B), which is the difference between the photon energy and kinetic energy of the photoelectron. This is known as the photoelectric effect and was first discovered by Heinrich Hertz in 1887 (1). Albert Einstein managed to explain this phenomenon in 1905, which resulted in a Nobel Prize in Physics in 1921 (2).

In photoelectron spectroscopy, we take advantage of this effect. In this thesis, we measure carbon 1s ionization energies of hydrocarbons in the gas phase using very intense X-rays. This is called X-ray photoelectron spectroscopy, often abbreviated to XPS. Traditionally, XPS has been used to find the chemical composition of a sample. The inner-shell ionization energy of an element is affected by its chemical environment, and XPS is

therefore sometimes referred to as *electron spectroscopy for chemical analysis* or ESCA (3; 4).

To obtain ionization energies with highest possible accuracy, it is necessary to use light with very special properties and a detector device where the kinetic energies of the photoelectrons can be measured with high precision. Synchrotron radiation may possess the desired properties and is produced at facilities with highly advanced equipment. From the 1950s until today, the instruments at the synchrotron radiation facilities have developed and improved significantly (5). The improvements enable the scientists to obtain experimental data with higher spectral resolution, and hence learn more about the sample than ever before.

When the carbon 1s photoelectron spectrum has been measured, we need a tool to analyze, interpret and understand the data. Quantum mechanical calculations have shown to be such a tool, and may provide many important properties of the system; molecular geometries, frequencies, thermochemical data, chemical shifts, and transition state energies to mention a few. From the calculated frequencies, vibrational line progressions associated with carbon 1s ionization at each unique carbon atom are computed and fitted to the experimental spectrum in a least-squares routine. Since our sample is measured at very low pressures, it is modelled theoretically using a single molecule.

1.2 Aims and structure of the thesis

The overall aim of the present work is two-fold. On one hand, theoretical methods and procedures have been developed to be applied in present and future analyses of complex carbon 1s photoelectron spectra. On the other, accurate C1s ionization energies and important chemical properties have been determined and explored for a series of alkenes and alkynes by using XPS and theoretical modeling.

A positively charged species is produced in a carbon 1s ionization. However, there are other chemical processes that also produce species with a positive charge. One example where this is the case is the proton addition to the unsaturated bond of an alkene. An example where a partial positive charge is added to one of the unsaturated carbons, is the electrophilic addition of a hydrogen halide like for instance HCl. It has previously been shown that shifts in core-ionization energies and activation energies in addition of hydrogen halides to ethene, propene and 2-methylpropene are approximately linearly correlated (6). This suggests that the energy changes involved in the addition of a hydrogen halide may be dependent on the same molecular properties as do the core-ionization energies.

In the present thesis, the validity of this conjecture is explored for larger and more complex olefins. In these investigations, the corresponding alkynes

have also been included to facilitate a comparison of alkenes and alkynes with respect to chemical reactivity in electrophilic addition reactions. Moreover, earlier studies revealed excellent correlations between enthalpies of protonation and C1s energies (7; 8; 9). We consider protonation to represent a gas-phase model for the rate determining electrophilic attack in solution, and the present work includes enthalpies of protonation as a reactivity parameter. The results from this study can be found in paper IV.

As the size or chain length of the alkene or alkyne increases, the number of possible stable geometries the hydrocarbon may possess through rotation about internal carbon–carbon single bonds increases rapidly. These possible geometries are known as conformational isomers or conformers. The total number of unique carbons associated with a compound is essentially given by the product of the number of conformers and the number of carbon atoms in unique chemical environments in a single conformer of the molecule. Each of the different carbons may provide a C1s energy that is different from all the other C1s energies of the molecule. In this way, the number of individual contributions to the C1s spectrum increases, which in turn makes the spectral analysis more difficult and complex.

Rather than viewing this as a problem, one might ask if it is possible to resolve the conformers and explore their properties by means of XPS. Recent studies have shown that XPS in combination with theory is indeed a useful tool to investigate conformational properties of hydrocarbons containing heteroatoms (10; 11).

However, the alkenes and alkynes explored in the present work do not contain heteroatoms that can induce large shifts in C1s energy. As indicated above, this makes the conformational analysis more complex and sometimes even impossible. In order to resolve and assign accurate C1s energies to each unique carbon atom, it is necessary to introduce external information to the spectral analysis. One way to accomplish this, is to compute accurate chemical shifts in C1s energy and apply these shifts as constraints in the spectral analysis. In this thesis, the conformational properties of most of the alkenes and alkynes possessing two or more conformers have been explored using this technique. These results are presented in paper II and III.

To be able to compute shifts in C1s ionization energies accurately, it is necessary to obtain an overview of the theoretical methods that are suitable for this purpose. To achieve this, C1s shifts from theory have been compared with the corresponding shifts determined from XPS. From these comparisons, the C1s shift accuracy of a range of ab initio and density functional theory (DFT) methods has been established. These results can be found in paper I.

The rest of the thesis is structured in the following manner. Chapter 2 describes how a synchrotron radiation facility is built up and works, and provides some important properties of synchrotron radiation as well as details about how the experiment is performed. In chapter 3, the main theoreti-

cal methods used in this thesis are presented, in addition to computational details and other theoretical aspects. Chapter 4 presents factors that affect the vibrational lineshapes associated with C1s ionization at each carbon site, and describes how the data analysis is performed. Chapter 5 provides an overview of the results, and concluding remarks as well as suggestions for further work are given in chapters 6 and 7, respectively.

Chapter 2

Experimental

This chapter describes shortly how a typical synchrotron radiation facility is built up, how synchrotron radiation is produced, important properties of synchrotron radiation, and finally how the experiment is carried out. The experimental data used in this thesis has been measured at MAX-lab (12) in Lund, Sweden, and Advanced Light Source (ALS) (13) in Berkeley, USA, over the period 1998 to 2008. Both are examples of third-generation synchrotron radiation facilities, and are in principle using the same components. They produce exceptionally bright light which in turn provide spectra with ultrahigh resolution. A description of synchrotrons and their radiation properties can be found in the book by Attwood (14). Parts of the discussion below are based on information provided by this book.

2.1 Synchrotron radiation

A charged particle travelling on a curved trajectory emits electromagnetic radiation. This is the foundation of synchrotron radiation. To describe shortly how a typical synchrotron radiation facility is built up and how it produces synchrotron radiation, MAX-lab is used as an example. An overview of the laboratory is given in Figure 2.1.

The light is generated in a process which consists of several steps. First, electrons are generated from an electron source called the electron gun. These electrons are accelerated by a linear accelerator before they are injected into the first MAX ring, MAX I. Here, the electrons are further accelerated and sent through undulators and bending magnets to produce light which is monochromatized to remove all unwanted wavelengths, and finally used for experiments. However, the range of photon energy and intensity at MAX I is for carbon 1s measurements. The accelerated electrons in the MAX I ring are injected into the larger MAX II ring. Here, the electrons are further accelerated to near the speed of light. These electrons are sent through undulators or wigglers to produce extremely intense light. After

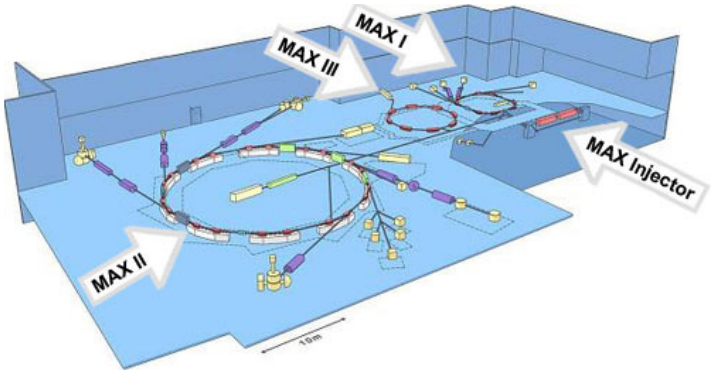

Figure 2.1: The MAX-laboratory. The figure is taken from Ref. (12), with permission.

monochromatization of the radiation, it is used for experiments at the end station of the beamlines surrounding the MAX II ring. MAX III is a third ring producing third-generation light which is operated for production of UV light.

Beamline I411 is located at the MAX II ring. The first device at I411 is the undulator which has periodic magnetic structures with relatively weak magnetic fields (14). The periodicity causes the electron to experience a harmonic oscillation as it moves in the axial direction. This results in a motion which is characterized by small angular excursions called undulations. Because of these weak magnetic fields, the amplitude of this undulation is forced to be small giving a narrow radiation cone. As a result, we obtain a radiation with small angular divergence and relatively narrow spectral width. This light also has a high level of polarization, wide tunability in wavelength by monochromatization, and high brilliance and brightness.

Synchrotron radiation is produced as the electrons pass through the undulators. The energy loss of the electron beam to synchrotron radiation is replenished with a radio-frequency accelerator. This is a cavity with an axial electric field which is oscillating at the frequency of arrival of sequential electron bunches (14). The radiation coming out of an undulator must then be spectrally filtered by a monochromator which further narrows the relative spectral bandwidth and remove all wavelengths that are not used in the experiment.

2.2 The experiment

At the end of the beamline, we find the end station where the experiments are carried out. The photoelectrons from the sample are measured in a hemispherical analyzer illustrated in Figure 2.2.

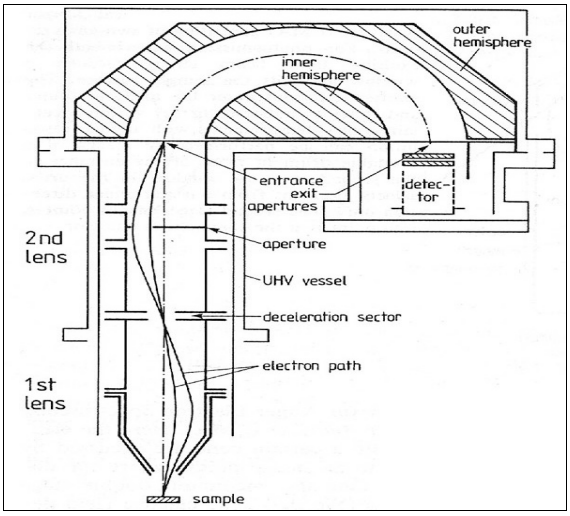

Figure 2.2: A layout of a hemispherical electron energy analyzer.

The analyzer consists of two entrance lenses that focus incoming electrons onto the entrance aperture and finally an electron detector. The electron trajectory is between two metallic hemispheres, where the entrance and exit apertures are circular, producing a circular image. The electrons that converge, are the ones that are deflected through an angle of 180 degrees. The following equation shows that the energy resolution depends on the analyzer.

$$\frac{\Delta E}{E} = \frac{x_1 + x_2}{2r} + \alpha^2 \tag{2.1}$$

The variable r equals $\frac{a+b}{2}$ where a and b are the radii of the hemispheres. x_1 and x_2 are the radii of the entrance and exit aperatures. The angle α is the maximum deviation of the electron trajectory with respect to the normal to the entrance aperture.

The electrons passing the entrance aperture experience immediately a change in the electric field when they enter the hemispherical part of the analyzer. The hemispherically-shaped electrodes have a negative and a positive charge which repulses and attracts, respectively, the incoming electrons. While the electrode nearest the centre of the hemisphere has a positive charge, the other one farthest away has a negative charge. Electrons with high kinetic energy will not be affected by the electric field to the same extent as the low-energy electrons. Thus, the low-energy electrons will be detected close to the centre of the hemisphere, and the high-energy electrons will be detected farther away from the centre. In this way, as the electrons

are counted and plotted against the kinetic energy of the photoelectrons, a photoelectron spectrum is generated.

An experimental session begins with adjustments of the experimental parameters until a spectrum with optimal resolution is measured. Often, a test measurement of xenon is performed for energy calibration of the spectrometer. A manifold is mounted and used to introduce the samples into the gas cell. The samples, in most cases a liquid, are usually obtained commercially. About 2 mL of the liquid sample is transferred to a glass tube and mounted to a manifold. The air inside the glass tube and manifold is removed by pumping the closed system. This is done by freezing the liquid to a solid sample using liquid nitrogen.

After heating the solid sample back to liquid, the vapour pressure of the sample is usually enough to obtain a measurable pressure of about 10^{-6} mbar inside the analyzer. A higher pressure in the gas cell gives a higher spectral intensity, but because of scattering effects and charge accumulation in the gas cell, this decreases the resolution of the spectrum. After completing the measurements of a sample, the instrument is prepared for a new measurement by pumping the manifold and analyzer. Sometimes, the manifold is heated to remove the sample attached to the walls inside.

Typical parameters that are adjusted in between each experiment are the pass energy, analyzer slit opening, energy range, step energy, time per step, number of sweeps per experiment run, energy of the incoming monochromatized light, undulator gap, monochromator slit opening, and pressure inside the analyzer. The pass energy is the energy of the electrons as they pass through the analyzer (usually 20 eV), while the step energy is the energy interval in which the electron intensity is not recorded at the detector (usually 10 meV). The undulator gap is the distance between the two permanent magnets in the undulator, and the mono-slit is the exit-slit of the monochromator.

With synchrotron radiation, the photon energy accuracy is not high. This means that the apparent photon energy may change from one day to another with a given monochromator setting due to instabilities or imperfections of the instrument. One effect that contributes to measurement errors, is charge accumulation in the gas cell during a measurement. Thus, to find the accurate ionization energies, it is necessary to include an internal standard or calibrant for which the ionization energy is well known. The calibrant is mixed together with the sample during the measurement to obtain a spectrum where both components are included. A satisfactory calibrant should have its peak close to the compound of interest, but not overlapping. The calibrant should also be available at a low cost. In carbon 1s measurements, both CO_2 and CF_4 fulfill these requirements.

Chapter 3

Theoretical methods

A carbon 1s photoelectron spectrum often contains a lot of information. When a C1s spectrum has been measured, we want to understand and explain the different features of the data. A molecule with many chemically unique carbon atoms often provides a spectrum with several overlapping peaks, each of them having a complex fine structure.

To be able to resolve and describe all the spectral features, one needs a powerful tool. Theoretical methods and calculations have shown to fulfill this need. With the help from theory, it is possible to generate vibrational lineshapes associated with C1s ionization at each unique carbon site. It is also possible to compute molecular properties like proton affinities, activation energies in electrophilic addition of hydrogen halides, conformational stabilities, and accurate ionization energy differences or chemical shifts, to mention a few.

In this chapter, the theoretical methods applied in this thesis are presented in a qualitative manner, and equations and expressions are therefore reduced to a minimum. For a more detailed description of quantum chemistry methods and spectroscopy, several books are available (15; 16; 17; 18; 19; 20).

3.1 The Schrödinger equation

Electronic structure methods use the laws of quantum mechanics as the basis for their computations. Quantum mechanics states that the energy and other related properties of a molecule or an atom may be obtained by solving the time-independent and non-relativistic Schrödinger equation first introduced by Erwin Schrödinger in 1926.

$$\hat{H}\Psi = E\Psi \tag{3.1}$$

Equation 3.1 is a special case of the general time-dependent equation

$\hat{H}\Psi = i\hbar\frac{\partial\Psi}{\partial t}$. In this thesis, all computations have been performed using equation 3.1, where $\hat{H}$ is the energy operator called the Hamiltonian and E is the energy of the system. Ψ is known as the wavefunction, and all the information about a system is described by this function. The Hamiltonian consists of a kinetic ($\hat{T}$) and potential ($\hat{V}$) energy operator.

$$\hat{H} = \hat{T} + \hat{V} \tag{3.2}$$

However, exact solutions to Equation 3.1 are very difficult to obtain for any but the smallest systems. This problem is solved by applying the Born Oppenheimer approximation (17), which exploits the mass difference between the electrons and nuclei. The foundation for the approximation is that the electrons will reorientate instantaneously according to the motion of the much heavier nuclei. This leads to a separation of the nuclear and electronic parts of the wave function, and therefore, the nuclei can be viewed as fixed in position and the Schrödinger equation is solved for the electrons in the static electric potential arising from the nuclei in that arrangement.

To solve the electronic problem, many different methods have been developed with different degree of sophistication, and a brief description of the methods used in this thesis is given in the following sections. Furthermore, an expansion of the harmonic oscillator functions is the most popular approximation to represent the potential energy term $V_i(R)$, which is defined by the electronic energy of state i and nuclear repulsion energy at nuclear coordinates R. However, this approximation only provides satisfactory descriptions of the lower vibrational states.

An important property of electrons (or other fermions with half-integer spins) is that no two electrons may occupy the same quantum state simultaneously. This is known as the Pauli's exclusion principle, and means that the electronic wavefunction for two electrons must be antisymmetric upon interchange of spin and spatial coordinates.

3.2 The Hartree-Fock approximation

The Hartree-Fock method (21; 22) is often used as a starting point for other more accurate methods (see Section 3.3). Since Hartree-Fock describes most molecules qualitatively correct and is relatively little computationally demanding, it is a very popular method.

Within the Hartree-Fock approximation, the atom is described as a system consisting of N independent electrons where the motion of each electron is described in the average field of the nucleus and all the other $N-1$ electrons. The electronic wave function is obtained from variational minimization of the electronic energy with respect to the spatial orbitals[1], leading to

[1] An orbital is a wave function for a single electron.

the Hartree-Fock equations. Molecular orbitals are expressed from a set of atomic orbitals and the Hartree-Fock equations are solved iteratively until self-consistency is achieved.

There are two types of Hartree-Fock approximations, restricted (RHF) and unrestricted (UHF) Hartree-Fock. In restricted Hartree-Fock, all the electrons except those occupying open-shell orbitals are forced to occupy doubly occupied spatial orbitals, each orbital containing two electrons of opposite spin. In open-shell unrestricted Hartree-Fock, separate spatial orbitals are used for the spin up and spin down electrons.

3.3 Post-Hartree-Fock methods

Since the Hartree-Fock method is a mean-field theory and does not consider the instantaneous electrostatic interactions between electrons, it is clear that this method ignores electron correlation. Perturbation theory (PT) provides an alternative systematic approach to find the correlation energy. The application of PT to a system composed of many interacting particles, is generally called many-body perturbation theory (MBPT). Because it is necessary to find the correlation energy of the ground state, one takes the zero-order hamiltonian $\hat{H}^{(0)}$ from the Fock-operators of the Hartree-Fock method. This procedure is called Møller-Plesset perturbation theory (MPPT).

The HF ground-state wavefunction ϕ_0 is an eigenfunction of the zero-order hamiltonian $\hat{H}^{(0)}$, which is a sum of one-electron Fock operators with an eigenvalue $E^{(0)}$ given by the sum of the orbital energies of all the occupied spin orbitals. The perturbation $\hat{H}^{(1)}$ is given by Equation 3.3.

$$\hat{H}^{(1)} = \hat{H} - \hat{H}^{(0)} \tag{3.3}$$

Here, $\hat{H}$ is the exact electronic hamiltonian. The first correction to the ground state energy is given by second-order perturbation theory as shown in Equation 3.4.

$$E^{(2)} = \sum_{J \neq 0} \frac{< \phi_J | \hat{H}^{(1)} | \phi_0 >< \phi_0 | \hat{H}^{(1)} | \phi_J >}{E^{(0)} - E_J} \tag{3.4}$$

The inclusion of the second-order energy correction is designated MP2. In general, bond lengths based on MP2 are in excellent agreement with experiment for bonds involving hydrogen while multiple bond lengths are predicted poorer.

MP3 (23; 24) and MP4 (25) include third- and fourth-order energy corrections to the energy respectively. MP3 is usually not sufficient to handle cases where MP2 does poorly, and the improvements over MP2 are often

too small compared with the additional computational cost. MP4, however, does successfully address many problems MP2 and MP3 can not handle.

The coupled cluster (CC) levels of theory also treat electron correlation, and often provide results with even greater accuracy than do the MPn methods (26; 27; 28; 29). They iteratively include effects of single and double substitutions (CCSD), and can optionally include triples and quadruples. In coupled cluster approaches, each class of excited configurations is included to infinite order. This is accomplished with the usage of an exponential excitation operator shown in Equation 3.5.

$$\Psi_{CC} = e^{\hat{T}}\phi_0 = \left[1 + \hat{T} + \frac{\hat{T}^2}{2!} + \frac{\hat{T}^3}{3!} + \cdots\right]\phi_0 \tag{3.5}$$

Here, ϕ_0 is the HF determinant for an N-electron system, and $\hat{T} = \hat{T}_1 + \hat{T}_2 + \hat{T}_3 + \cdots + \hat{T}_N$. $\hat{T}_1$ produces singly excited determinants, $\hat{T}_2$ doubly excited determinants, and so on. For the CCSD(T) method, a CCSD calculation is followed by a contribution due to triple excitations ($\hat{T}_3$) from perturbation theory (30).

3.4 G3

The Gaussian-3 (G3) theories are general procedures for computing the total energies of molecules at their equilibrium geometries (31). A G3 calculation consists of several calculations that are performed step-wise. The first step is a Hartree-Fock optimization and frequency calculation. The next step is a full geometry optimization at the MP2 level of theory, followed by a series of MP4 and QCISD(T) single point calculations with larger basis sets. This method, as well as the G1 and G2 methods (32; 33; 34), have been developed in an attempt to determine thermochemical quantities accurately.

3.5 Density functional theory (DFT)

Density functional theory (DFT) is based on the work of Fermi and Thomas (35; 36), as well as Hohenberg, Kohn and Sham (37; 38). Methods based on DFT have steadily gained popularity the last couple of decades, and achieve often greater accuracy than Hartree-Fock theory at only a modest increase in computational cost. These methods do so by including some of the effects of electron correlation in a computationally less costly manner than do traditional correlated methods. The electron correlation is computed via general functionals[2] of the electron probability density, $\rho(\vec{r})$.

[2] A functional is a function on a vector space V, usually of functions.

$$\rho(\vec{r}) = |\psi(\vec{r})|^2 \tag{3.6}$$

For a system of N electrons, $\rho(\vec{r})$ denotes the total electron density at a particular point in space r. The electronic energy E is said to be a functional of the electron density, and is denoted $E[\rho]$. Apart from the nuclear-nuclear repulsion, all terms included in the electronic energy are functions of the electron probability density.

The DFT functionals partition the electronic energy into kinetic energy, electron-nuclear interaction, Coulomb repulsion, and exchange-correlation accounting for the remainder of the electron-electron interaction. The exchange-correlation energy is itself divided into separate exchange and correlation components in most DFT formulations. The major problem with DFT is that the exact functionals for exchange and correlation are not known. Furthermore, there are no systematic ways to improve the accuracy of a calculation. The only way to do this is to use different exchange and correlation functionals.

A wide variety of functionals have been defined, and they are generally distinguished by the way they treat the exchange and correlation components. Local exchange and correlation functionals involve only the values of the electron spin densities, and gradient-corrected functionals involve both the values of the electron spin densities and their gradients. The Slater exchange functional and Vosko, Wilk and Nusair (VWN) correlation functional are examples of local functionals, and the Becke 1988 exchange functional as well as the Lee, Yang and Parr (LYP) correlation functional are examples of gradient-corrected functionals.

3.5.1 B3LYP

Hybrid functionals are another class which defines the exchange functional as a linear combination of Hartree-Fock, local, and gradient-corrected exchange terms, which is then combined with a local and/or gradient-corrected correlation functional. The most frequently used hybrid functional is the Becke three-parameter formulation B3LYP (39). The exchange-correlation energy for this functional is expressed in Equation 3.7 (16).

$$E_{XC}^{B3LYP} = (1-a)E_X^{LSD} + aE_{XC}^{\lambda=0} + bE_X^{B88} + cE_C^{LYP} + (1-c)E_C^{LSD} \tag{3.7}$$

Here, a, b and c are 0.20, 0.72 and 0.81 respectively. These are three empirical parameters chosen such that the atomization and ionization energies, proton affinities and some total energies are optimally reproduced (40). E_X^{LSD} is the local spin density exchange energy, $E_{XC}^{\lambda=0}$ is the exchange-correlation energy where the coupling strength parameter λ is zero, E_X^{B88} is

the Becke88 exchange energy, E_C^{LYP} is the Lee-Yang-Parr correlation energy and E_C^{LSD} is the local spin density correlation energy.

3.6 Basis sets

The wavefunctions or orbitals are constructed from a set of mathematical functions called a basis set, and must be specified in an electronic structure calculation. The larger the basis set, the more accurately the orbitals are approximated by imposing fewer restrictions on the locations of the electrons in space. However, more computational resources are necessary as the size of the basis set increases.

A standard basis set consists of a number of atomic orbitals or basis functions. An atomic orbital can be approximated by basis functions, which are linear combinations of primitive Gaussian functions of the form $P(x, y, z)e^{-\alpha x^2}$. Here, $P(x, y, z)$ is any polynomial in cartesian coordinates and α is the orbital coefficient.

Since an atomic orbital can be represented by more than one basis function, this provides flexibility to the basis set. Therefore, the basis sets are called double-, triple-, quadruple-zeta, etc. depending on the number of basis functions for each atomic orbital. Molecular orbitals are represented as linear combinations of atomic orbitals, and this is known as the LCAO approximation. It is also possible to add polarization functions which are Gaussian functions having one quantum number of higher angular momentum than the atomic valence orbitals. In this way, polarization functions also add flexibility within the basis set, often providing a better description of chemical bonds. One can also add diffuse functions to the basis set, which are Gaussian functions that more accurately describe the parts of orbitals that are distant from the atomic nuclei. Anions are one example where it is particularly important to add diffuse functions.

In this thesis, a triple-zeta basis set has been the default choice in the calculations, meaning that each valence atomic orbital is represented by three basis functions. This basis set was augmented by one set of polarization functions for each atom; a p-set for hydrogen and a d-set for carbon.

3.7 Hole-state calculations

When an atom or molecule is core-ionized, a core hole is created. It is not easy to model the core hole explicitly since the highly excited state is subject to variational collapse. However, there are several approximate descriptions of the core hole. One of them is the equivalent-cores method where the core-ionized atom with nuclear charge Z is replaced by a isovalent valence-ionized atom with a closed-shell core and a nuclear charge of $Z + 1$.

However, this approximation does not predict changes in bond lengths and angles correctly.

A better alternative is the 1-electron effective core potential (ECP) (41). This method, which is very efficient computationally, models the effect of the core hole on the valence electrons and represents the core hole and core electrons using pseudopotentials. The ECP is usually tabulated in the literature as parameters of the expansion shown in Equation 3.8.

$$ECP(r) = \sum_{i=1}^{M} d_i \times r^{n_i} \times 10^{-\zeta_i \times r^2} \tag{3.8}$$

M is the number of terms in the expansion, d_i is a coefficient for each term, r denotes the distance from the nucleus, n_i is a power of r for the ith term, and ζ_i represents the exponent for the ith term. To specify the ECP for a given atomic center, it is necessary to include the number of core electrons that are substituted by the ECP, the largest angular momentum quantum number included in the potential, and number of terms in the polynomial Gaussian expansion shown in Equation 3.8. In this thesis, the ECP has been the default method to model the effect of the core hole on the valence electrons.

To test the capability or limitations of the ECP approximation, DALTON (42) calculations were performed at the Hartree-Fock level of theory using an explicit core hole. The chemical shifts from these calculations were compared with the corresponding Hartree-Fock shifts based on the ECP. The results from these calculations are presented in paper I.

3.8 The extended Koopmans' theorem (EKT)

There are two contributions to the chemical shift ΔI. One of these contributions is ΔV, which is the effect of the electric potential at the core of the carbon and is defined by the ground-state charge distribution. An accurate estimate of ΔV can be determined as shown in the following.

One way to find the contribution from the initial state to the ionization energy, is to equate the initial-state effect V to the negative of the electrostatic energy of a core electron. However, this is an over-simplification because of the neglect of the kinetic energy and exchange interactions of the electrons. An alternative way to estimate V, is to approximate the initial-state effect by the negative of the orbital energy of the core electron. Koopmans' theorem shows that within the Hartree-Fock approximation, the energy needed to remove an electron without rearrangements of the spectator electrons is given by $-\epsilon_c$, where ϵ_c is the core-orbital energy as shown in Equation 3.9.

$$I = -\epsilon_c \tag{3.9}$$

In section 4.2, we will see that $I = V - R$. In this expression, R is the final state charge redistribution. When the rearrangement of the spectator electrons is excluded (R), we obtain $I = V$ which finally gives the expression $V = -\epsilon_c$. Koopmans' theorem is a one-electron model and is true under the condition that electron correlation may be neglected and there are no relaxations of the spectator electrons during the ionization. This means that the same orbitals are describing both the initial and final states. Koopmans' theorem often provides too high ionization energies, and the difference between experiment and theory based on Koopmans' theorem has a tendency to increase with increasing ionization energies. The reason for this is the neglect of the final state effect ΔR (see Equation 4.3).

It has been shown that $-\Delta\epsilon_c$ provides inaccurate estimates of ΔV due to the neglect of electron correlation in the initial state. Hence, it was necessary with an extension of Koopmans' theorem which took into account the influence of valence-electron correlation in addition to the wave nature of the core electrons. This is called the extended Koopmans' theorem (EKT) (43) and is expressed in Equation 3.10.

$$\Delta V \approx -\Delta\epsilon_c + (\Delta U^{VCI} - \Delta U^{HF}) \tag{3.10}$$

In this equation, $\Delta\epsilon_c$ is the difference in initial-state core-orbital energies, and ΔU is the difference in electrostatic energy of a unit positive charge at the two nuclei that are being compared. The superscripts HF and VCI are abbreviations for Hartree-Fock and valence-correlated levels of theory respectively. Equation 3.10 is valid when the core orbitals are well-localized or close-to-degenerate.

3.9 The Franck-Condon principle

When a molecule is core ionized, the nuclei are subjected to a change in Coulombic force because of the redistribution of electronic charge. This involves a change in the molecular potential energy surface as the electronic state changes during the core ionization. These simultaneous electronic and vibrational transitions are known as vibronic transitions. The nuclei respond to this change by vibrating or swinging about their original position. The energy required for these vibrations to occur is absorbed by the molecule from the photons used to core ionize the molecule. In this way, photoelectrons will be detected with somewhat lower kinetic energies, providing vibrational progressions at higher ionization energies.

The vibrational structure of an electronic transition is explained by the Franck-Condon principle which states that, because the nuclei are so much more massive than the electrons, an electronic transition takes place very much faster than the nuclei can respond. In the Franck-Condon picture, the intensity of the transition is directly proportional to the squared magnitude of the transition dipole moment, μ_{fi}^2, shown in Equation 3.11.

$$|\mu_{fi}|^2 = |\mu_{\epsilon_f,\epsilon_i} S(\nu_f, \nu_i)|^2 \tag{3.11}$$

Here, $\mu_{\epsilon_f,\epsilon_i}$ is the electronic transition dipole moment, and $\mathrm{S}(\nu_f, \nu_i)$ is the overlap integral between the vibrational states of the initial and final electronic states. The squared overlap integral $|S(\nu_f, \nu_i)|^2$ is known as the Franck-Condon factor for the transition. The greater the overlap of the vibrational state wavefunction in the upper electronic state with the vibrational wavefunction in the lower electronic state, the greater the intensity of that particular simultaneous electronic and vibrational transition.

The Franck-Condon principle is illustrated in Figure 3.1 for a harmonic oscillator in a one-dimensional case of a diatomic molecule. In the figure, the molecular potential energy is plotted as a function of the internuclear distance, ν and ν' are the sets of vibrational quantum numbers of the initial and final electronic state, respectively, and R_e and R'_e are the equilibrium bond lengths of the initial and final electronic state, respectively.

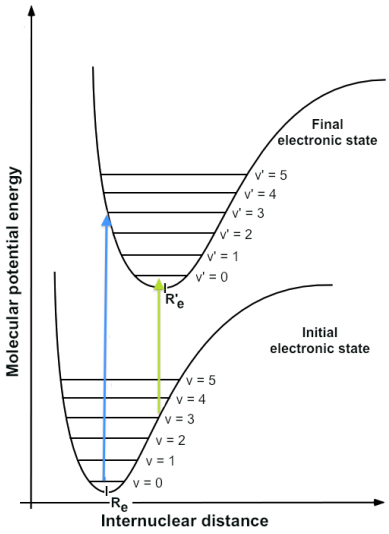

Figure 3.1: An illustration of the Franck-Condon principle for a harmonic oscillator in a one-dimensional case of a diatomic molecule. ν and ν' denote the vibrational quantum numbers for the initial and final electronic state, respectively.

The upper curve is typically displaced to the right relative to the lower curve since electron excitations often introduce more antibonding character into the molecular orbitals. The transition from $\nu = 0$ to $\nu' = 3$ (blue arrow) is an example of a fundamental progression since the transition is starting in the ground vibrational state of the lower electronic state. The figure also illustrates the transition from $\nu = 3$ to $\nu' = 0$ (green arrow) as an example. For both illustrated transitions, the internuclear distance is the same in the final state as it was intially, and such transitions are called vertical. Immediately after the electronic transition, the molecule starts to vibrate at an energy corresponding to the intersection. An increase in the relative displacement of the initial and final state potential curve leads typically to a broadening of the vibrational structure.

3.10 Vibronic coupling

There are cases where deviations from the Franck-Condon picture occur. Vibronic coupling is one such case, and this phenomenon occurs when two close-lying electronic states couples via the excitation of a vibrational mode. Furthermore, this is an example where the Born-Oppenheimer approximation breaks down. The vibronic coupling affects the vibrational profile, and this effect is often observed as a broadening of the carbon peak. Ethyne is an example where this effect is significant, and in this case the antisymmetric C-H stretching mode is excited due to vibronic coupling (44). Symmetric doubly bonded hydrocarbons with equivalent carbon atoms have also been subject to vibronic coupling, and benzene is one example for this class of symmetric compounds (45).

One problem in core ionization of symmetric molecules with equivalent atoms, is whether the carbon 1s hole can be treated as completely localized (diabatic) or as delocalized (adiabatic) with weak or strong electronic coupling (β). For a number of molecules, it has been found that the vibronic structure is well predicted by a localized model (46; 47; 48; 49; 50; 51). For ethyne, however, such a model is not sufficient to describe the vibronic structure in the spectrum. The ground state of the core-ionized ethyne is far from degenerate with a splitting between the $1\sigma_u^{-1}(^2\Sigma_u^+)$ and $1\sigma_g^{-1}(^2\Sigma_g^+)$ states of about 100 meV (52), and it has been shown that this large splitting is better described by a delocalized model and vibronic coupling (44). Furthermore, this splitting can be explained from the significant overlap between the diabatic degenerate core orbitals, and the degree of overlap increases as the carbon-carbon distance decreases.

In most cases, a peak is split into two peaks with equal intensity and a split equal to $2\beta < L, \upsilon | R, \upsilon >$. Here, $< L, \upsilon | R, \upsilon >$ is the vibrational overlap integral between the vibrational wavefunctions when the core hole is localized on the left atom (L) and those when it is localized on the right

atom (R). The electronic coupling integral β is common to all vibrational levels, and depends strongly on the distance between the carbon atoms. β is typically 10 meV for adjacent singly-bonded carbons, and about 30 meV for adjacent doubly-bonded carbons.

In this thesis, the effect of vibronic coupling has been accounted for in the least-squares fit analysis by splitting all the diabatic lines of the unsaturated carbons into two identical vibrational profiles. Since the splitting between the two profiles is used as a parameter in the fit, it is possible to determine the effect of vibronic coupling experimentally. The symmetrical molecules where significant vibronic coupling have been observed are trans-2-butene, trans-3-hexene, 2-butyne and 3-hexyne.

3.11 Computational details

All the theoretical calculations were performed in the Gaussian 03 and 09 set of programs (53; 54). Electrostatic potentials and orbital energies were computed at the HF/TZP and MP2/TZP levels of theory, and the G3 method was used to compute proton affinities, conformational populations and other thermochemical data. Activation energies in HCl addition to double and triple bonded hydrocarbons were calculated using the B3LYP hybrid functional together with the following basis: saturated parts of the hydrocarbons were described with atom-centered Gaussian-type functions contracted to triple-ζ quality (55) and augmented by polarization functions (56), leading to C: [5s, 3p, 1d] and H: [3s, 1p], referred to as the TZP basis. For the unsaturated carbon atoms, this set was augmented by diffuse s,p functions with exponents α_s=0.04561 and α_p= 0.03344. Similarly, HCl was described by H: TZP + diffuse s function (α_s=0.0709); Cl: valence TZ [6s,5p] (57) plus diffuse even-tempered (s,p) (α_s=0.0600; α_p=0.0314) and a doubly-split polarization set. All polarization functions were taken from Pople (Ref. (56)), either "6-311G(2d)" (Cl) or "6-311G(d,p)" (C, H).

The TZP basis was used with B3LYP to obtain geometries and vibrational frequencies, and the frequencies were calculated within the harmonic oscillator approximation. Both TZP and cc-pVTZ were used in combination with the Hartree-Fock, MPn (n=2, 3 and 4), CCSD and CCSD(T) methods to compute chemical shifts. A wide range of DFT methods was also used to compute shifts in combination with the same basis sets, in addition to the cc-pVDZ and cc-pVQZ basis sets. The DALTON code (42) was applied to compute explicit core-hole shifts at the HF/TZP and HF/cc-pVTZ levels of theory.

The frequency output files for both ground and final states were used as inputs in G2FC (Gaussian-to-Franck-Condon) (58) to compute the vibrational line progressions. A2FC (Asym-to-Franck-Condon) (59) is another program similar to G2FC. While G2FC uses cartesian coordinates, A2FC

uses internal coordinates. The ASYM40 software (60) was applied to transform Cartesian force constants from *ab initio* calculations to a force field having internal coordinates, and these results were used as input to the A2FC calculation. Both G2FC and A2FC identify the individual normal modes and their frequencies in the ground and final states. The programs also allow for individual scaling of the frequencies, perform Franck-Condon analysis for the totally symmetric modes, and provides computation of change in normal coordinate (Δq).

Very accurate calculations for methane show that the present level of theory exaggerates the contraction in C-H bonds that takes place during the ionization of sp^3 carbons by 0.3 pm (61) and ethane (51). Correspondingly for the sp^2 carbons, theory exaggerates the C-H bond contraction during ionization by 0.2 pm, as judged from very accurate calculations for ethylene (45; 62). Hence, in the G2FC and A2FC analyses mentioned above, the calculated C-H bond lengths at the ionized sp^3 and sp^2 carbon atoms were increased by 0.3 and 0.2 pm respectively. For the sp carbons, the C-H bond lengths were increased by 0.3 pm.

Furthermore, calculated harmonic frequencies are slightly higher than the frequencies found experimentally (51; 63; 64). To correct for this effect in G2FC and A2FC, all the calculated vibrational energies were scaled by a factor of 0.99, the C-H stretching modes on the core-ionized sp and sp^3 carbon atoms were scaled by 0.95 (65), and the corresponding modes on the sp^2 carbons were scaled by 0.96 (45; 62).

Chapter 4

Data analysis and lineshape functions

In carbon 1s photoelectron spectroscopy, the vibrational line progression associated with core ionization at each unique carbon atom has a given shape. The spectral analysis as well as different physical processes influencing the lineshape are described in this chapter.

4.1 Data analysis

Each carbon atom in a hydrocarbon has a vibrational line progression associated with carbon 1s ionization at that particular site, and these lines are applied in the analysis of the carbon 1s photoelectron spectrum. In order to make them, this must be done in several steps. The first step is to calculate the molecular geometries, normal modes, and vibrational frequencies of both the initial and core-ionized states. From the frequencies, the lines can be calculated using a program called G2FC (58) or A2FC (59) (see Section 3.11 for details).

When the experimental spectrum is measured and all the lines are calculated, different broadening factors or lineshape functions are convoluted (Fourier transform) with the lines and fitted to the experimental spectrum in a least-squares routine using the Igor Pro software (66; 67). The intensities and carbon 1s ionization energies are plotted along the ordinate and abscissa respectively, as shown in Figure 4.1 where 2-butyne (paper IV) is used as an example.

In this figure, both carbon 1 (C1) and carbon 2 (C2) are convoluted with a Gaussian, Lorentzian and an asymmetric line due to post collision interaction (PCI) to the total lineshape. The Gaussian width represents the instrumental broadening due to the uncertainty of the energy analyzer and monochromator. The Lorentzian width (Γ_L) is related to the lifetime of the core hole (τ) through equation 4.1.

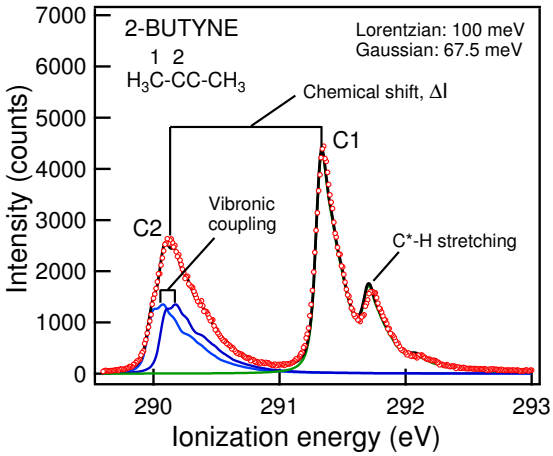

Figure 4.1: The fitted carbon 1s photoelectron spectrum of 2-butyne. The red circles represent the experimental spectrum, the black solid line the overall theoretical spectrum, and the blue and green solid lines the theoretical atom-specific lineshape profiles. The figure is adapted from paper IV.

$$\tau \cdot \Gamma_L \approx \hbar \tag{4.1}$$

This equation is similar to the Heisenberg's uncertainty principle where $\hbar$ equals $h/2\pi$ and h is Planck's constant. The lifetime broadening of a carbon 1s line is about 100 meV, which corresponds to a lifetime of about $7\text{x}10^{-15}$ seconds or 7 femtoseconds of the core hole using equation 4.1.

When core photoelectron spectroscopy is carried out on light elements such as carbon, the Auger process dominates the secondary decay. In a normal Auger process, the normal Auger process is preceded by a core electron being ejected into continuum by an incoming photon. This is followed by a decay of a valence electron into the core, which causes an ejection of a valence electron into continuum. The second-ejected electron is called an Auger electron.

When the Auger electron moves faster than the photoelectron, the Auger electron will catch up with the photoelectron and pass it. Consequently, the photoelectron experiences an effective charge of +2 instead of +1 from the ionized atom or molecule which is left behind, leading to a retardation of the photoelectron. The Auger electron, however, experiences a charge of +1 instead of +2 after the passage of the photoelectron which speeds up the Auger electron even more. This process is called post-collision interaction (PCI) and is illustrated in Figure 4.2 (68). The PCI effect provides an asymmetric line which is amplified on the low kinetic energy side or high

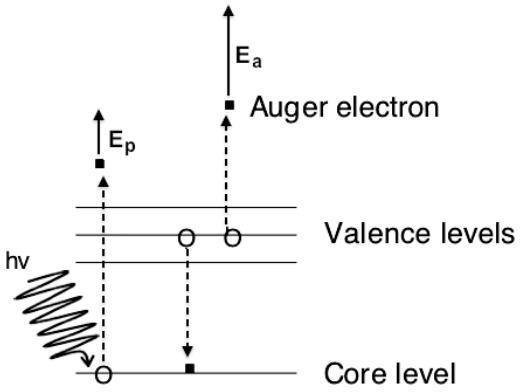

Figure 4.2: An illustration of a post collision interaction (PCI). The kinetic energy of the Auger electron (E_a) is greater than the kinetic energy of the photoelectron (E_p).

ionization energy side of the spectrum.

The asymmetry parameter can be found from equation 4.2, where $\epsilon_{PE} = \frac{E_{KIN}}{27.21\ eV/H}$ and $\epsilon_{Auger} = \frac{250\ eV}{27.21\ eV/H}$. Here, the mean kinetic energy of the Auger electron is 250 eV. E_{KIN} is the kinetic energy of the photoelectron ionized from the molecule in eV, while ϵ_{PE} and ϵ_{Auger} are the kinetic energies of the photoelectron and Auger electron in atomic units (au), respectively.

$$Asymmetry = \frac{1}{\sqrt{2}}\left(\frac{1}{\sqrt{\epsilon_{PE}}} - \frac{1}{\sqrt{\epsilon_{Auger}}}\right) \tag{4.2}$$

Equation 4.2 is an approach by van der Straten et al. (68) which models the PCI effect. This means that the asymmetry increases with decreasing kinetic energy of the photoelectron and increasing kinetic energy of the Auger electron.

4.2 Other broadening parameters

For highly symmetric molecules like ethyne, the core levels can not be regarded as atomic in character. As mentioned in Section 3.10, the core-hole states of the molecule occur in pairs of nearly degenerate states of *gerade* and *ungerade* symmetry where the internuclear distance between the carbon atoms is connected with the *gerade-ungerade* energy splitting. The magnitude of this splitting is determined by an electronic coupling integral β and a vibrational overlap integral specific to each vibrational state. As illustrated

in Figure 4.1, the diabatic line representing C2 of 2-butyne is split into two diabatic lines due to vibronic coupling. However, it is important to note that vibronic coupling is also possible when non-equivalent carbons accidentally have degenerate core levels. More details about vibronic coupling are given in Section 3.10.

The chemical shift is defined as the difference in C1s ionization energy between two carbon atoms with different chemical environment, and this is exemplified in Figure 4.1 for C1 and C2 of 2-butyne. The C1s shift does not affect a single atom-specific vibrational lineshape, but the whole spectrum which is the sum of all the different lineshapes. In carbon 1s photoelectron spectroscopy, the chemical shift ΔI can be separated into two contributions, ΔV and ΔR. ΔV is the effect of the electric potential at the core of the carbon and is defined by the ground-state charge distribution. ΔR is the effect of electronic and geometric relaxation in the final state. The quantities are related as shown in Equation 4.3.

$$\Delta I = \Delta V - \Delta R \tag{4.3}$$

ΔR can be calculated by subtracting ΔI from ΔV, where ΔI is experimental XPS data and ΔV is calculated using the extended Koopmans' theorem (EKT) described in section 3.8.

The lineshape is also dependent on the vibrations that occur in the core ionization. By providing vibrational structure to the total lineshape, this molecular behaviour affects the C1s photoelectron spectrum. The C^*-H stretching progression of C1 on the high-energy side of the 2-butyne spectrum is prominent, as shown in Figure 4.1. This process follows the Franck-Condon principle, as described in Section 3.9.

Figure 4.3 is an illustration of the shake-up process. An incoming photon excites a core electron to continuum, whereas some of the energy is used to excite or shake up a valence electron to a higher valence level. This shake-up process is an electron transfer from the highest occupied molecular orbital (HOMO) to the lowest unoccupied molecular orbital (LUMO). The shake-up process occurs more frequently as the molecular orbital energy differences decreases.

Unsaturated molecules have a higher tendency of shake-up compared to saturated molecules because of the small energy difference between the HOMO and LUMO (69; 70). The effect of shake-up can be observed as a peak with relatively low intensity at typically 5-10 eV higher ionization energies than the carbon 1s photoelectron spectrum. However, the overall core photoelectron spectrum does not lose or gain intensity due to shake-up since the extra shake-up intensity at 5-10 eV higher ionization energies reduces the intensity accordingly at the lower ionization energies in the spectrum. Hence, this may be an important reason why some carbon peaks have lower intensities than others.

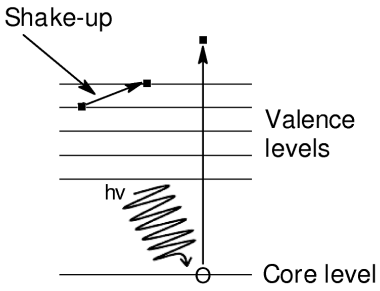

Figure 4.3: An illustration of the shake-up process.

Doppler broadening is another broadening factor which originates from the effect of the motion and rotation of molecules or atoms on the photoelectrons. For instance, if a molecule travels with a certain velocity at the same time as a C1s electron is ejected from the molecule in the same direction as the molecular direction, the measured kinetic energy of the photoelectron will be higher than if the molecule was static. The opposite is the case if the photoelectron is ejected in the opposite direction of the travelling direction of the molecule. However, this factor has a relatively small influence on the broadening of the spectra. Since both the Doppler and instrument broadening are random in nature (normal distribution), both are well described by a Gaussian function.

Chapter 5

Results

5.1 Accurate calculation of chemical shifts

The main goal of the present work was to explore the relationship between carbon 1s ionization energies and chemical reactivity in electrophilic addition reactions of alkenes and alkynes. However, for some of the molecules included in this study, the agreement between the experimental and model C1s spectrum was far from satisfactory. The reason for this turned out to be the following. For hydrocarbons with few carbon atoms in the chain, the carbon 1s photoelectron spectrum is usually well resolved and the chemically different carbon atoms are fairly easy to assign. However, as the size of the hydrocarbon increases, the complexity of the spectrum increases correspondingly. This is particularly the case when two or more conformers contribute to the carbon 1s photoelectron spectrum. In such cases, the total number of different carbons is dramatically higher since it equals the product of the number of unique carbons in the molecule and the number of conformers. To reduce the number of degrees of freedom in the analysis and secure satisfactory, credible and reproducible results of such complex spectra, accurate theoretical predictions of the chemical shift in C1s ionization energies turn out to be a prerequisite.

Paper I explores the accuracy in C1s shifts predicted from *ab initio* and density functional theory (DFT) methods in combination with the Dunning TZP and cc-pVTZ basis sets. The included *ab initio* methods are Hartree-Fock (HF), Møller-Plesset many-body perturbation theory (MPn with n = 2, 3 and 4), and coupled cluster (CCSD and CCSD(T)). The hybrid density-functional B3LYP was used for comparison with the *ab initio* methods. For the DFT part of the work, analogous calculations with the cc-pVDZ sets were carried out with the cc-pVTZ in an extrapolation procedure toward the complete basis-set limit. Additional tests were performed for selected functionals with the large cc-pVQZ basis. In all cases, the optimized geometries and zero-point vibrational energies were taken from B3LYP/TZP

calculations. A database of 77 experimental carbon 1s ionization energies was prepared, covering linear and cyclic alkanes and alkenes, linear alkynes, and methyl- and fluoro-substituted benzenes. All the experimental shifts relative to methane were compared with those from theory, and statistical parameters were calculated to obtain an overview of the shift accuracy of the different theoretical methods.

5.1.1 The *ab initio* methods

In Figure 5.1, error distributions of various electronic structure methods are presented. In combination with the TZP basis, the coupled cluster and MP4 methods are predicting highly accurate shifts.

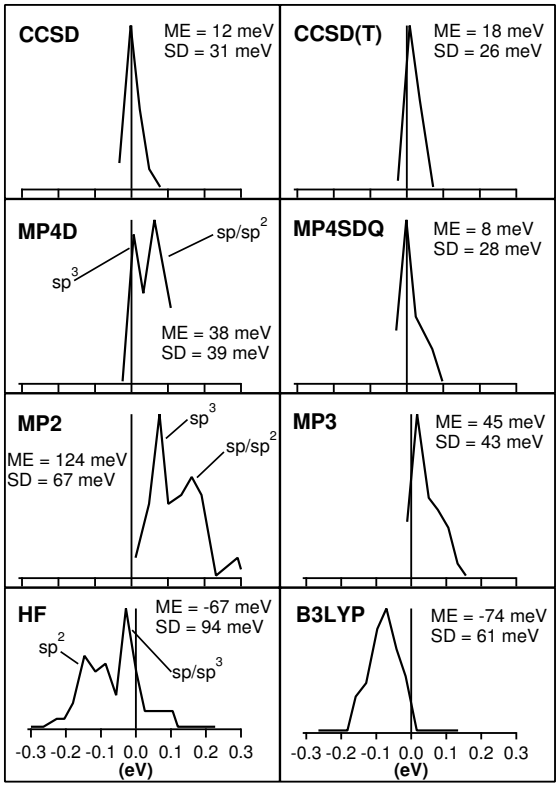

Figure 5.1: Error distributions expressed in mean errors (ME) and standard deviations (SD) in carbon 1s ionization energy shifts, as computed with various electronic structure methods using the TZP basis and an effective 1-electron core potential (ECP) describing the ionized core. The figure is adapted from paper I.

All calculations described above use an effective 1-electron core potential (ECP) to simulate the effects of the ionized core on the valence electrons. However, this approximation does not include a self-consistent-field-optimized singly-occupied orbital. To explore the possible errors this approximation might give rise to, all the chemical shifts in the database were calculated at the Hartree-Fock/TZP level of theory using an explicit and self-consistent core-hole description. These results were compared with a similar set of calculations using the ECP and the same molecular geometries and basis set. For the sp^3 and sp^2 carbons, there were no significant differences between the ECP and explicit core-hole calculations. For the sp carbons, however, the ECP errors were notable larger. One possible reason for these large errors is the strongly induced orbital relaxation effects in the core orbital of sp carbons. On the other hand, the short C-C distance in triple bonds also implies a stronger tendency of delocalizing the core hole over the pair of sp carbons, which is not well described at the Hartree-Fock level of theory. Hence, the conclusion is that the ECP model describes the core hole well for most of the systems. Assuming that the ECP errors are transferable between electron-structure methods, the ECP shifts calculated at a different level of theory can be corrected for this.

To investigate the effect of hybridization in more detail, the 77 chemical shifts were divided into sp, sp^2 and sp^3 subgroups. Statistical parameters were calculated for each group and compared with the parameters deduced from the whole data set. For example, for many of the methods included in the study, the errors were significantly smaller when the data set was reduced to a sp^3 data set. At the CCSD(T)/TZP level of theory, the RMSD value, which is a measure of the error between the least-squares fit line and the plotted values, is reduced from 24 meV when all hybridizations are included, to 18 meV when only sp^3 shifts are included. The RMSD value of 18 meV is further reduced to 14 meV when the larger cc-pVTZ basis set is used. These differences are comparable with the estimated uncertainties in the experimental data, indicating that the CCSD(T) calculations are describing these shifts within the experimental uncertainties. This is a strong indication that, at least for sp^3 carbons, the estimated uncertainties in the experimental shifts of 10-20 meV is correct.

5.1.2 The DFT methods

One disadvantage by using advanced *ab initio* methods to calculate chemical shifts is the computational cost, in particular for the larger molecules. Hence, it is desirable to utilize less expensive methods that provide shifts with comparable accuracy. Density functional theory (DFT) may provide such a method. Even though the hybrid density functional B3LYP predicts the shifts relatively poorly, as shown in Figure 5.1, there are many other existing functionals that may be appropriate. Available functionals include

combination functionals in which one exchange and one correlation functional are combined in the calculation, pure functionals, and hybrid functionals. To explore the shift qualities of the different functionals, single-point calculations including 156 combination functionals, 30 hybrid functionals, and 8 pure functionals were performed in combination with the TZP, cc-pVDZ, and cc-pVTZ basis sets. All computed shifts were compared with the same database of experimental shifts that were used for the *ab initio* methods.

The root mean squared error (RMSE) is a statistical parameter that reflects the accuracy of the functionals and includes both systematic and random errors. In Figure 5.2, the RMSE values of selected combination functionals are presented.

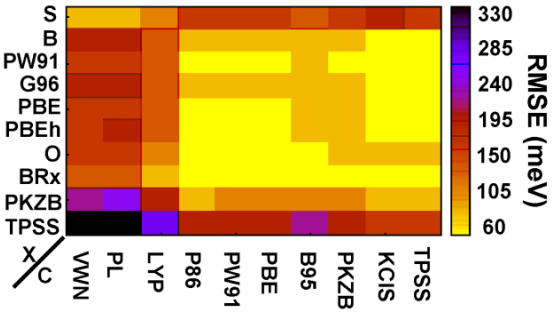

Figure 5.2: A plot of the RMSE values between experimental shifts and the chemical shifts predicted by selected exchange (X) and correlation (C) functionals using the TZP basis and experimental shifts. The figure is adapted from paper I.

To reduce the amount of data, the functionals were chosen based on differences between them. Hence, only 100 of a total of 156 combination functionals are presented in figure 5.2. In general, there are greater variations in the RMSE values among the exchange functionals (X) than among the correlation functionals (C), showing that the shifts are more sensitive to the choice of exchange functional than correlation functional. The plot also shows that the BRx exchange functional stands out as the one with generally highest accuracy. The lowest RMS errors in the 55-60 meV range are about the double of the corresponding MP4SDQ/TZP and CCSD(T)/TZP errors, 29 and 32 meV respectively.

Shifts were also calculated using selected pure and hybrid functionals in combination with the TZP basis, and the computed shifts were compared with the experimental shifts. The RMS errors of these functionals are presented in Figure 5.3, where five combination functionals are included for

comparison.

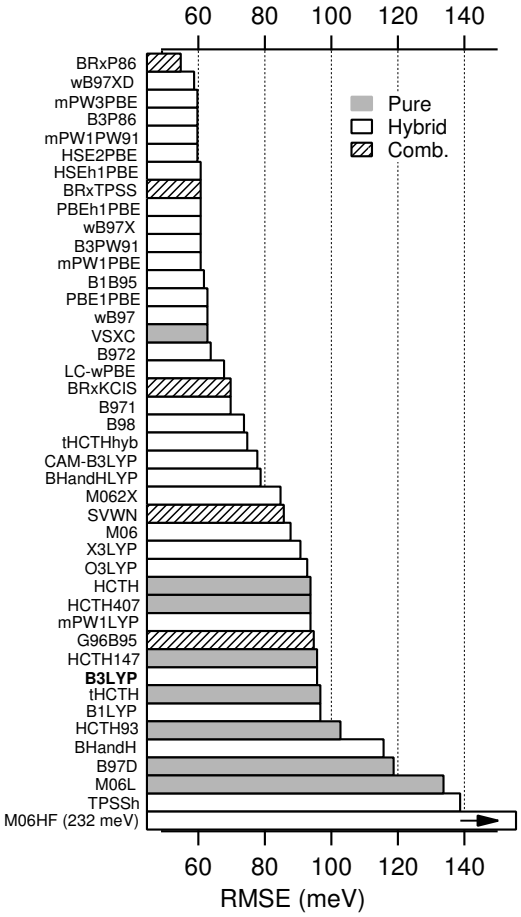

Figure 5.3: RMS errors (RMSE) between the chemical shifts predicted by combination, pure and hybrid functionals using the TZP basis and experimental shifts. The figure is adapted from paper I.

The figure shows that more than half of the functionals have RMSE values below 80 meV, and that the M06HF hybrid functional is significantly worse than the rest. However, the BRx exchange functional in combination with the P86 correlation functional provides excellent shifts, and has the lowest RMSE among all the selected functionals. With a RMSE of 96 meV, B3LYP is only mediocre.

5.2 Conformational analysis

An unsaturated hydrocarbon may possess two or more conformers, which are defined as all possible and stable geometries a molecule may obtain by rotation about single bonds. The γ-CH/π interaction is one of several factors that determine the relative stability between conformers of hydrocarbons with unsaturated bonds. Even though this interaction is regarded as the weakest among hydrogen bonds (71; 72; 73), it is often found in peptides, indicating that it has an impact on the 3D structure of proteins (74).

Experimental methods such as IR/Raman (75; 76; 77; 78), microwave spectroscopy (79; 80), NMR (81), electron momentum spectroscopy (82), and gas-phase electron diffraction (83) have traditionally been used for conformational analysis. The last couple of decades, IR/UV double- and triple-resonance spectroscopies have also been applied to investigate conformational problems (84; 85; 86; 87; 88; 89). A common goal for these studies has been to identify and sometimes quantify the different conformers by observing their signal intensities, and the experimental results are often supplemented with theoretical calculations.

The last decade, theory-assisted XPS has been found to reveal conformational properties of hydrocarbons containing hetero atoms such as oxygen, nitrogen and fluorine (10; 11). As we will see later in this section, this is only possible when C1s ionization energies or vibrational lineshapes are significantly different between conformers at least at one particular carbon site.

In this thesis, the conformational properties of the alkenes and alkynes presented in Table 5.1 have been investigated. On one hand, we study the conformational properties of unsaturated hydrocarbons where there are no large chemical shifts induced by heteroatoms. On the other, we explore the limitations of using theory-assisted XPS for conformational analysis.

Table 5.1: An overview of the alkynes and alkenes whose conformational properties have been studied in this thesis, and the number of their nondegenerate conformers (N_C), varying from 2 to 41 (90).

Molecule	Formula	N_C
1-Pentyne	$HC{\equiv}CCH_2CH_2CH_3$	2
4-Methyl-1-pentyne	$HC{\equiv}CCH_2CH(CH_3)_2$	2
1-Hexyne	$HC{\equiv}CCH_2CH_2CH_2CH_3$	5
2-Hexyne	$H_3CC{\equiv}CCH_2CH_2CH_3$	2
1-Heptyne	$HC{\equiv}CCH_2CH_2CH_2CH_2CH_3$	14
1-Butene	$H_2C{=}CHCH_2CH_3$	2
1-Pentene	$H_2C{=}CHCH_2CH_2CH_3$	5
Trans-2-pentene	$H_3CCH{=}CHCH_2CH_3$	2
1-Hexene	$H_2C{=}CHCH_2CH_2CH_2CH_3$	14
Trans-2-hexene	$H_3CCH{=}CHCH_2CH_2CH_3$	5
Trans-3-hexene	$H_3CCH_2CH{=}CHCH_2CH_3$	4
1,5-Hexadiene	$H_2C{=}CHCH_2CH_2CH{=}CH_2$	10
1-Heptene	$H_2C{=}CHCH_2CH_2CH_2CH_2CH_3$	41

Since the number of parameters in a least-squares fit of the theoretical model with the experimental spectrum increases rapidly with the number of conformers, it is sometimes necessary to introduce constraints to the fit in order to secure credible and reproducible results. One way to do this, is to freeze relative energy positions or shifts between different carbons according to theoretical predictions. With the results from the extensive comparison of theoretical and experimental C1s shifts at hand, we are now in position to choose the appropriate theoretical methods to compute these shifts accurately.

5.2.1 1-Pentyne and 4-methyl-1-pentyne

1-Pentyne, investigated in paper II, is the smallest triply bonded hydrocarbon with the ability to possess conformers in its ground state. The two possible conformers of 1-pentyne, *anti* and *gauche*, are illustrated in Figure 5.4 and can be obtained by rotation about the C3-C4 bond. The dotted $CH\cdots\pi$ distances have been computed at the G3 level of theory.

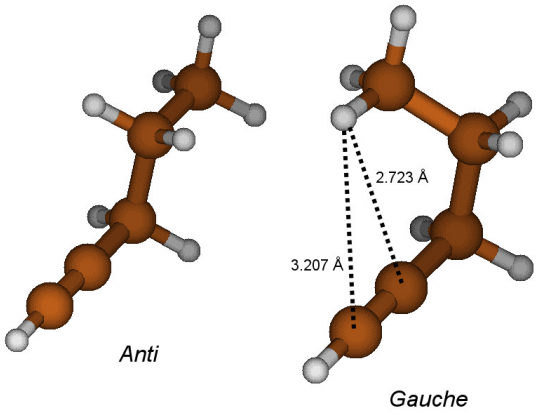

Figure 5.4: The two conformers of 1-pentyne. The figure is adapted from paper II.

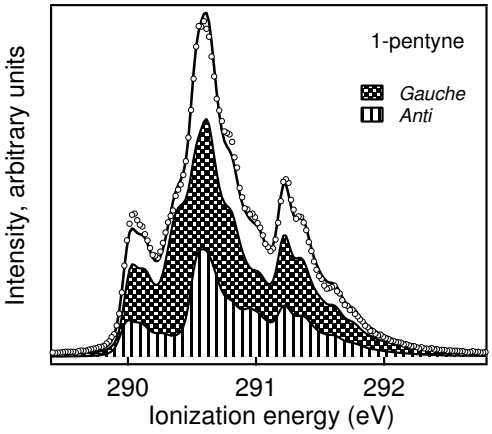

Figure 5.5: The experimental C1s photoelectron spectrum of 1-pentyne (circles) is shown together with theoretical fitting models (solid line) based on a model that takes into account both *anti* and *gauche* conformers. The contributions from the two conformers are shown as shaded areas. The figure is adapted from paper II.

The distribution of the *anti* and *gauche* conformers of 1-pentyne has been a source of controversy for decades, where the *anti* population has ranged from 27% to 46% (77; 91; 92; 93; 83). The analysis from XPS and theory yields 29% *anti*, in agreement with microwave spectroscopy (93) and

electron diffraction studies (83).

The analysis of the 1-pentyne spectrum was performed as follows. 1-Pentyne has five unique carbon atoms, and when both conformers are taken into account, the amount of different carbons is doubled to ten. Consequently, a total of ten vibrational profiles were calculated to include both conformers in the analysis. The ten profiles were fitted to the spectrum in a least-squares routine, and the result is shown in Figure 5.5.

Here, the five *anti* profiles are summed into one shaded area and the five *gauche* profiles summed into one. The conformational population was determined from these intensity areas. The analysis shows that carbon 1 (C1) constitutes the low-energy peak, carbon 3 (C3) the high-energy peak, whereas C2, C4 and C5 are grouped together in the main peak with highest intensity. The figure shows a very good agreement between the theoretical model spectrum (black solid line) and the experimental one (circles).

The carbons in the main peak are close in ionization energy. Consequently, to avoid unphysical and unreliable results, the intensity areas within each conformer were constrained to be the same, and some of the main peak carbons were energy-constrained according to chemical shifts from accurate theoretical predictions. As mentioned in section 5.1, the choice of theoretical method was based on a series of calculations where the computed chemical shifts were compared with the corresponding experimental shifts. Since the shifts computed at the CCSD(T)/cc-pVTZ level of theory were found to be the most accurate at the time of publication (94), they were applied in the analysis of the 1-pentyne spectrum.

From a comparison of each conformational pair of carbon atoms ($C1_{anti}$ vs $C1_{gauche}$ etc.), carbon 5 was found to be the only carbon atom with significantly different ionization energies and vibrational lineshapes. As mentioned earlier, these differences are crucial since they enable us to quantify contributions from *anti* and *gauche* conformers in the spectrum.

Finally, all vibrational profiles were fitted to the experimental spectrum with the restrictions described above. One of the parameters in the least-squares refinement was the relative amount of each conformer, which provided the possibility to determine the population and hence relative stability of the two conformers.

In paper III, the work from paper II was taken further and conformational properties of a number of alkenes and alkynes were explored, and most of the molecules were even larger than 1-pentyne. We have seen that XPS and theory can be used as a technique to identify and quantify the conformers of 1-pentyne. However, can this technique also be used for conformational analysis of alkenes as well as larger and even more complex systems than 1-pentyne? These are some of the questions that paper III attempted to answer.

4-Methyl-1-pentyne is one of the alkynes that are investigated in paper III. Like 1-pentyne, this alkyne is a triply bonded hydrocarbon with the

ability of possessing two conformers in its ground state. The structures of the *anti* and *gauche* conformers of 4-methyl-1-pentyne are illustrated in Figure 5.6. One particularly interesting property of this alkyne is the ability of the two methyl groups in the *gauche* conformer to participate in a γ-CH/π interaction.

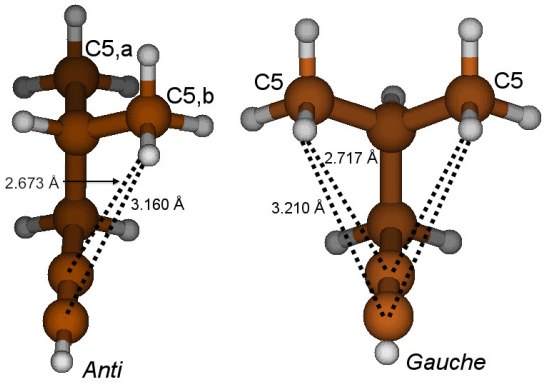

Figure 5.6: The conformers of 4-methyl-1-pentyne. The figure is adapted from paper III.

The photoelectron spectrum of 4-methyl-1-pentyne was analyzed using a different approach than the one used for 1-pentyne. Instead of including a vibrational profile for each unique carbon atom, the number of profiles was reduced based on similarities in shifts and profiles. As we will see, the analysis can be simplified by excluding all profiles that do not contribute with new information to the overall spectrum. This means that one profile is sufficient to describe both conformers at some of the carbon sites.

Furthermore, since the different carbon atoms of 4-methyl-1-pentyne are more separated in C1s ionization energy (larger range) and the C1s spectra have more structure than is the case for 1-pentyne, both spectra were fitted without using constraints from theoretical predictions on the C1s shifts.

The *anti* and *gauche* conformers of 4-methyl-1-pentyne have six and five unique carbon atoms respectively. A comparison of the shifts and profiles of the two conformers is given in Table 5.2.

The similarity of the vibrational profiles can be calculated from expression 5.1. Here, FC_{anti} and FC_{gauche} are the Franck-Condon vibrational lineshape functions convoluted with a Lorentzian function with full-width-at-half-maximum set to 100 meV of the *anti* and *gauche* profiles, respectively. This index is equal to 1 if the two profiles are identical and vanishes if the profiles have no overlapping intervals of non-zero intensity.

Table 5.2: The chemical shifts of the 4-methyl-1-pentyne conformers computed at the MP4SDQ/TZP level of theory. All shifts in eV relative to ethyne. The similarities between the vibrational profiles of each unique carbon atom are given in percentage, computed from Eq. 5.1. The table is adapted from paper III.

Carbon	*Gauche*	*Anti*	*Gauche-Anti*	% similarity between the *gauche* and *anti* profiles[a]
C1	-1.139	-1.140	0.001	99.9
C2	-0.598	-0.604	0.006	99.8
C3	-0.045	-0.050	0.005	99.8
C4	-0.536	-0.540	0.004	99.8
C5,a	-0.903	-0.724	-0.179	93.9
C5,b	-0.903	-0.914	0.011	99.7[b]

[a]Vibrational profiles calculated at the B3LYP/TZP level of theory.
[b]The similarity between the C5,a and C5,b profiles of the *anti* conformer is 93.5%.

$$\frac{\int FC_{anti} FC_{gauche} d\epsilon}{\sqrt{\int FC_{anti}^2 d\epsilon \int FC_{gauche}^2 d\epsilon}} \tag{5.1}$$

Because of similarities in shifts and profiles between the two conformers, only one of the conformers was needed to describe C1-C4 satisfactory, reducing the total number of profiles significantly. C5, on the other hand, was included for both conformers because of the prominent differences in both shifts and profiles. Due to symmetry, the C5 carbons of the *gauche* conformer are equivalent while the C5 *anti* carbons are different (C5,a and C5,b). Consequently, we must include one C5 profile for the *gauche* conformer and two C5 profiles for the *anti* conformer for a full description of this carbon atom in the C1s photoelectron spectrum.

However, it is important to note that this simplification is also possible for 1-pentyne. Since C5 is the only carbon with large differences in vibrational profiles and chemical shifts between the two conformers, C1-C4 are sufficiently described by only one of the conformers, reducing the number of profiles from 10 to 6. Within the reported uncertainty, this simplified approach provides the same population as the one obtained in paper II.

The least-squares fits of 4-methyl-1-pentyne is shown in Figure 5.7. From the intensity areas of the C5 and C6 profiles, the percentage population of the *anti* conformer of 4-methyl-1-pentyne was found to be 70±6%. In the literature, the *anti* and *gauche* population of 4-methyl-1-pentyne is limited

to theoretical predictions. Hence, XPS provides an experimental determination of the hitherto unknown conformational population.

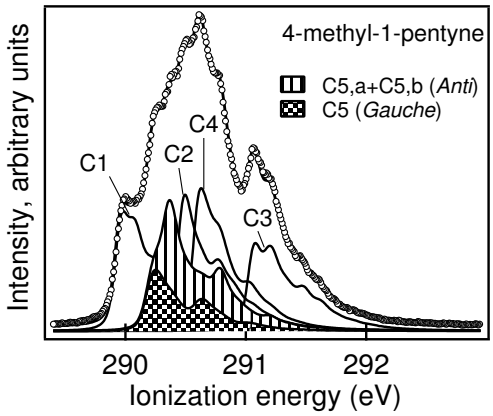

Figure 5.7: The carbon 1s photoelectron spectrum of 4-methyl-1-pentyne. The circles represent the experimental spectrum and the thick solid line is the overall theoretical spectrum. The thin solid lines represent the carbon atoms with the same vibrational profiles and chemical shifts for the pair of conformers, and the shaded areas represent the carbons with significantly different shifts and profiles for the two classes of conformers. The figure is adapted from paper III.

In a similar manner as 4-methyl-1-pentyne, the *anti* and *gauche* conformers of 2-hexyne have also been explored in paper III by means of XPS and theory. In this case, it is carbon 6 that provides significant differences in shifts and profiles for the two conformers. More details on this analysis, which reveals 30±5% *anti* conformers, can be found in paper III.

5.2.2 Limitations of XPS in conformational analysis

As mentioned earlier, the complexity of the analysis increases with the number of possible conformers. We have also seen that it is useful and often necessary to simplify the analysis by reducing the number of variables, which can be achieved by using constraints on the relative C1s energy positions predicted from accurate theoretical calculations. At the same time, however, this simplification also reduces the information about the conformational properties of the system. In this section, some limitations of XPS in conformational analysis are exemplified by 1-hexyne, 1-pentene and 1-butene.

1-Hexyne

1-Hexyne is an example where five conformers may be obtained by rotation about the C3-C4 and C4-C5 bonds, illustrated in Figure 5.8.

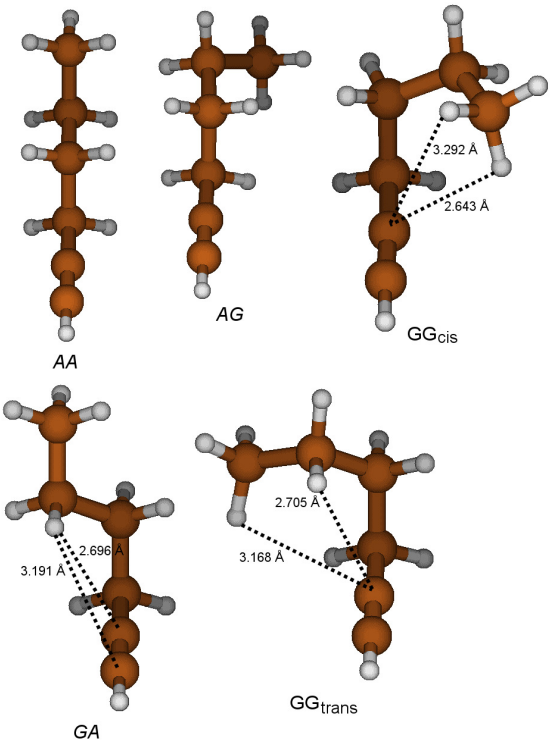

Figure 5.8: The structure of the five possible conformations of 1-hexyne. The figure is adapted from paper III.

Microwave and IR/Raman studies indicate that there are only four stable 1-hexyne conformers (95; 96; 97). The fifth conformer, GG_{cis}, was found to

be significantly higher in energy than the other conformers and is therefore ignored in the following analysis.

From the studies of 1-pentyne and 4-methyl-1-pentyne, we have seen that the carbon atoms with significant differences in shifts and profiles between the conformers are those with the possibility of having one of its hydrogen atoms pointing towards the π system. This is the case for carbon 5 of the *gauche* conformer of 1-pentyne. For 4-methyl-1-pentyne, C5 of both *anti* (C5,b) and *gauche* have this possibility.

In paper I, the MP4SDQ method in combination with the TZP basis set was found to predict the most accurate shifts in C1s energies. Hence, MP4SDQ/TZP shifts were applied in the analysis of the C1s spectrum of many of the alkenes and alkynes explored in paper III. In Table 5.3, all MP4SDQ/TZP shifts relative to ethyne are presented for the four 1-hexyne conformers. The table shows that C1, C2 and C4 have similar shifts for the different conformers, and C3 has a noticeable shift of 0.040 eV between the AG and GA conformers. However, as shown in the 1-hexyne spectrum in Figure 5.9, C3 has its own well-defined peak at approximately 291.2 eV. Although only one conformer is used to describe C3, the agreement between theory and experiment is satisfactory. This result indicates that the shift of 0.040 eV is too small to be observed in the spectrum.

Table 5.3: The chemical shifts of the four 1-hexyne conformers computed at the MP4SDQ/TZP level of theory. All shifts in eV relative to ethyne computed at the same level of theory. The similarities between the vibrational profiles of each unique carbon atom are given in percentage, computed from Eq. 5.1. The table is adapted from paper III.

Carbon	AA	AG	GA	GG_{trans}	Shift diff.[a]	Profile sim.[b]
C1	-1.135	-1.142	-1.130	-1.125	0.017	>99.8
C2	-0.599	-0.603	-0.595	-0.593	0.010	>99.8
C3	0.027	0.001	0.041	0.005	0.040	>99.6
C4	-0.684	-0.673	-0.673	-0.660	0.024	>99.9
	Group A		Group B			
C5	-0.668	-0.652	-0.850	-0.846	0.197	>94.2
C6	-0.687	-0.684	-0.773	-0.790	0.106	>98.1

[a]Largest shift difference.
[b]Least profile similarity (%). Vibrational profiles calculated at the B3LYP/TZP level of theory.

For C5 and C6, the four conformers were divided into two groups according to similarities in the shifts. The AA and AG conformers have comparable shifts, and so do the GA and GG_{trans} conformers. Similarly, the vibrational profiles have been compared for the different conformers. For

C1, all combinations of profiles provide a similarity close to 100%, which is also the case for C2, C3, C4 and C6. For C5, however, the smallest similarity is 94% (between AA and GA), notable smaller than the other carbon atoms. Due to similarities in shifts and profiles, these results are in accordance with placing the AA and AG conformers into one group, and the GA and GG_{trans} conformers into another. These groups are assigned as group A and B, respectively, as shown in Table 5.3.

Based on these results, the AA conformer was chosen to represent the group A conformers and the GA conformer to represent the group B conformers. As mentioned earlier, C1-C4 have similar shifts and profiles, and therefore can be sufficiently described by only one of the conformers. Since C5 and C6 are described by both AA and GA, we have reduced the number of profiles to eight.

Even though the number of parameters has become smaller due to similarities in shifts and profiles, some of the carbon atoms are still very close in ionization energy. To avoid obtaining unreliable and unphysical results, MP4SDQ/TZP shifts were computed and used as C1s energy constraints for these carbons. The least-squares fit of the 1-hexyne spectrum is shown in Figure 5.9.

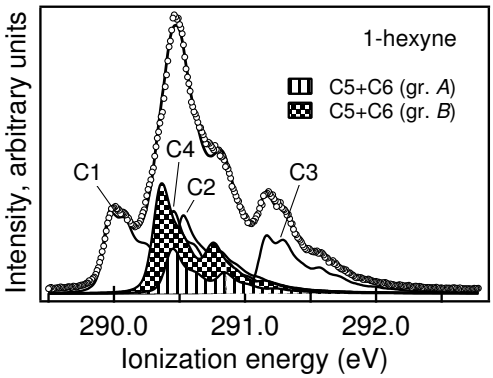

Figure 5.9: The carbon 1s photoelectron spectrum of 1-hexyne. The circles represent the experimental spectrum and the thick solid line is the overall theoretical spectrum. The theoretical spectrum of the sum of C5 and C6 of each group of conformers is shown with a shaded area. The figure is adapted from paper III.

From the intensity areas of the C5 and C6 profiles, the contribution of the group A conformers of 1-hexyne was found to be 28% (±8). To summarize, the limitation by using XPS to explore the 1-hexyne conformers is that we are not able to resolve all possible conformers, only groups of them. Each

group is characterized by the presence (or absence) of a 5-center γ-CH/π interaction.

1-Pentene

Five conformers of 1-pentene can be identified by rotation about the C2-C3 and C3-C4 bonds. Four of the conformers, numbered from *I* to *IV* in Figure 5.10, have been observed in microwave spectra (79) at room temperature (298K), suggesting that the fifth is only little populated. This was confirmed by MP2 calculations (79). Based on these results, conformer *V* was neglected in the analysis of the carbon 1s photoelectron spectrum of 1-pentene.

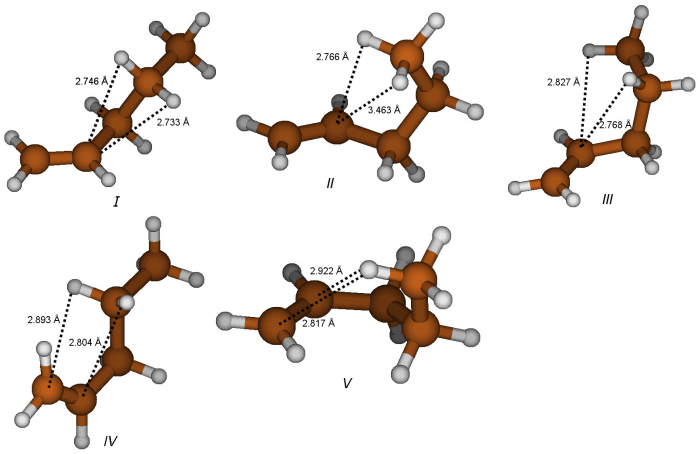

Figure 5.10: The structure of the five possible conformations of 1-pentene.

Like the alkynes, chemical shifts and profile similarities were calculated for all four conformers, and these results are summarized in Table 5.4.

In the case of C1, conformers *I* to *III* have about the same ionization energy. Conformer *IV*, however, has a significantly lower ionization energy by about 0.09 eV. This conformer has the characteristic 4-center CH/π interaction, and theoretical calculations performed in paper III strongly suggest that conformer *IV* is significantly higher in energy than conformers *I-III*. If conformer *IV* is important, a C1 split of about 0.09 eV would appear in the spectrum. Since we do not observe such a split, it is likely that conformer *IV* either has a small population, or the shift of 0.09 eV is overestimated. However, when the C1 vibrational profile of conformer *IV* is included in the analysis with a shift of 0.09 eV relative to C1 of conformer *I*, the fitted amount of conformer *IV* is found to be very small ($< 10\%$). This result suggests that conformer *IV* is very little populated.

Table 5.4: The chemical shifts of the four 1-pentene conformers computed at the MP4SDQ/TZP level of theory. All shifts in eV relative to ethyne computed at the same level of theory. The similarities between the vibrational profiles of each unique carbon atom are given in percentage, computed from Eq. 5.1. The table is adapted from paper III.

Carbon	*I*	*III*	*IV*	*II*	Shift diff.[a]	Profile sim.[b]
C1	-1.101	-1.100	-1.192	-1.100	0.092	>99.9
C2	-0.710	-0.730	-0.751	-0.711	0.041	>99.9
C3	-0.731	-0.726	-0.728	-0.716	0.015	>99.9
C4	-0.788	-0.782	-0.799	-0.775	0.024	>99.9
	Group A			Group B		
C5	-0.769	-0.789[c]	-0.777	-0.903	0.134	>94.0

[a]Largest shift difference.
[b]Least profile similarity (%). Vibrational profiles calculated at the B3LYP/TZP level of theory.
[c]Optimized geometry with a frozen C1-C2-C3-C4 dihedral.

Since the maximum difference in ionization energy between the conformers is only 0.04 eV with respect to C2, C3 and C4, these carbons are sufficiently described by only one of the conformers. C5 provides the largest shift between the two groups of conformers, 0.134 eV. This is a significant shift caused by the presence and absence of the 5-center γ-CH/π interaction in conformer *II* and *I*, respectively. This CH/π interaction is illustrated for conformer *II* in Figure 5.10 with a dashed line. Hence, this shift suggests that both conformer *II* and one of the group A conformers must be included in the analysis to describe C5 in the spectrum.

For C1-C4, all combinations of vibrational profiles for the conformers have similarities higher than 99.9%. For C5 the profile similarity is significantly smaller than the rest, 94.0%. Taking into account the shifts given in Table 5.4, these results suggest that conformers *I*, *III* and *IV* may be grouped together (group A) and conformer *II* has the potential of providing a unique XPS signal. Hence, in the 1-pentene fit shown in Figure 5.11, conformer *I* is used to describe C1-C4, and C5 is fit by two models; conformer *I* to represent the group A conformers and conformer *II* to describe group B.

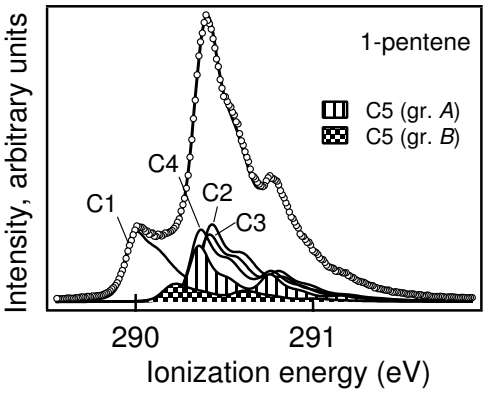

Figure 5.11: The experimental carbon 1s photoelectron spectrum (circles) of 1-pentene shown together with theoretical fitting models (thick solid lines). The thin solid lines represent the unique carbons with similar vibrational lineshapes and chemical shifts for a number of conformers, and the shaded areas represent carbons where the shifts and profiles are significantly different for two classes of conformers. The figure is adapted from paper III.

Due to significant geometrical distortion following ionization at C5 of conformer *III*, the C1-C2-C3-C4 dihedral angle was frozen in the geometry optimization at the B3LYP/TZP level of theory. This geometry was used to calculate the C5 profile and shift applied in the analysis described above. However, when the C5 final state geometry of conformer *III* was fully optimized at the same level of theory, the calculated MP4SDQ/TZP shift changed to -0.86 eV which is comparable with the corresponding shift of conformer *II* (-0.90 eV). The new profile was found to be significantly different from the other C5 profiles. For this reason, one can not expect a two-peak model for C5 to provide a faithful representation of the relative population of *I+IV* to that of *II+III*, or *I+III+IV* to that of *II*. The limited amount of structure in the C1s spectrum does not allow the introduction of separate fitting parameters for the intensities of *II*, *III* and *I+IV*. Hence, despite the excellent two-model fit, an estimate of the conformational group populations can not be provided from these results. A similar situation occurs for trans-2-hexene, 1-hexene, 1-heptene and 1-heptyne.

1-Butene

1-Butene is the smallest alkene with the ability to possess conformers. The two conformers of 1-butene, *anticlinal (AC)* and *synperiplanar (SP)*, are illustrated in Figure 5.12 and can be identified by rotating about the C2-C3 bond. While IR and NMR studies suggest that *SP* is the more stable con-

former (81; 75), a study based on electron momentum spectroscopy suggests that AC is the more stable one (82). Since theoretical energy differences between them are small and the statistical weight ratio W_{AC}/W_{SP} is two, the AC conformer is likely to dominate in the carbon 1s photoelectron spectrum.

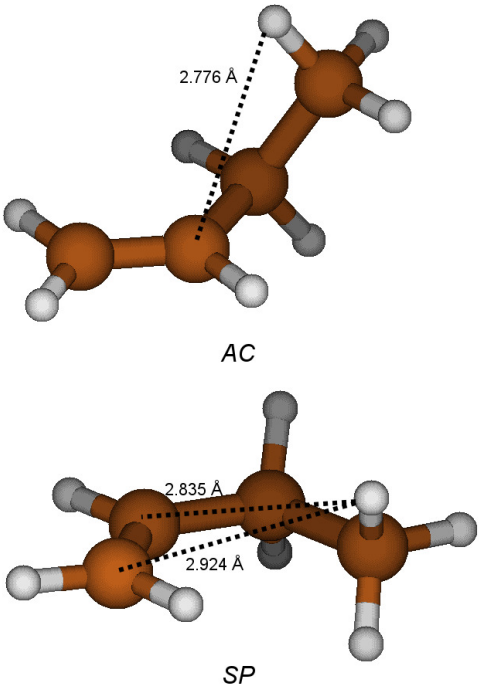

Figure 5.12: The structure of the two conformers of 1-butene. The figure is adapted from paper III.

In Table 5.5, vibrational profiles and chemical shifts of both 1-butene conformers are summarized. The table shows that C1, C3 and C4 have shifts above 0.03 eV and that all the profiles have similarities close to 100%. The major shift differences of C1 is presumably caused by the 4-center CH/π interaction in the SP conformer, illustrated with dashed lines in Figure 5.12.

Since C1 has a noticeable shift, there is reason to believe that this carbon must be included for both conformers in the analysis. However, vibrational profiles of the SP conformer describe the experimental spectrum about equally well as the AC profiles, and a combination of both conformers does not improve the overall fit of the spectrum appreciably. In the Supporting information of paper III, the AC conformer was chosen to describe the experimental 1-butene spectrum, as shown in Figure 5.13. Since each carbon has its own defined feature and energy position in the spectrum, in-

Table 5.5: The chemical shifts of the 1-butene conformers computed at the MP4SDQ/TZP level of theory. All shifts in eV relative to ethyne. The similarities between the vibrational profiles of each unique carbon atom are given in percentage, computed from Eq. 5.1. The table is adapted from paper III.

Carbon	*SP*	*AC*	*SP*-*AC*	% similarity between the *SP* and *AC* profiles[a]
C1	-1.113	-1.054	-0.059	99.9
C2	-0.671	-0.665	-0.006	>99.9
C3	-0.532	-0.570	0.038	99.9
C4	-0.679	-0.715	0.036	99.8

[a]Vibrational profiles calculated at the B3LYP/TZP level of theory.

tensities and energies were allowed to vary independently in the least-squares fit routine.

1-Butene is one of several examples where XPS cannot be used to determine conformational populations, and hence, reveal conformational properties of the system. Other examples are trans-2-pentene, trans-3-hexene and 1,5-hexadiene, all discussed in more detail in the Supporting information of paper III.

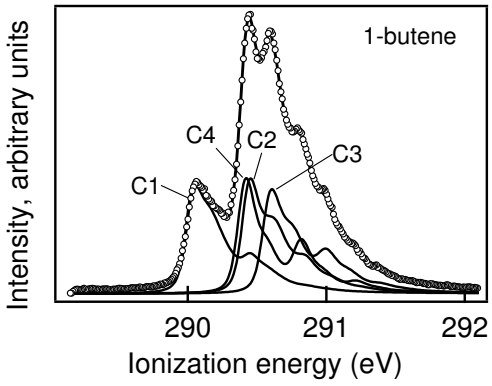

Figure 5.13: The carbon 1s photoelectron spectrum of 1-butene. The circles represent the experimental spectrum, the thick solid line the overall theoretical spectrum, and the thin solid lines the theoretical atom-specific lineshape models. The figure is adapted from paper III.

5.2.3 Conformational populations from theory

In paper II and III, conformational populations determined from XPS are compared with the corresponding theoretical predictions. 1-Pentyne, 4-methyl-1-pentyne and 2-hexyne are examples of molecules that possess only two conformers and facilitates a direct comparison of the XPS results with theory. One important motivation to do such comparisons, is to establish an overview of theoretical methods that are suitable for predicting relative conformational stabilities.

Table 5.6 gives an overview of the percentage population of the *anti* conformer of 1-pentyne, 4-methyl-1-pentyne and 2-hexyne, as calculated at various levels of theory (298K) from differences in Gibbs free energies, and as measured by XPS. The uncertainties of the XPS results are estimated from the statistics of the fit and the sensitivity of the result to variations in the fitting model. While B3LYP predicts too high *anti* populations, the MP2, G3 and CCSD(T) numbers are in very good agreement with the XPS results. As shown in the table, counterpoise corrections (CP) (98) have been included in the CCSD(T) calculations to account for basis-set superposition error (BSSE). In general, paper III shows that BSSE is not important in the comparisons between the experimental and theoretical results.

Table 5.6: The percentage population of the *anti* conformer[a] of 1-pentyne and 4-methyl-1-pentyne, and 2-hexyne, as computed at different levels of theory (298K) from differences in Gibbs free energies, and as measured by carbon 1s photoelectron spectroscopy (XPS).

	1-Pentyne	4-Methyl-1-pentyne	2-Hexyne
B3LYP/TZP	41	76	43
MP2/TZP	26	70	25
G3	33	68	33
CCSD(T)+CP/TZP[b]	34	73	32
XPS	29±3	70±6	30±5

[a] % *gauche* population: 100% - % *anti* population.

[b] Thermoanalysis from MP2+CP/TZP plus anharmonicity correction.

5.3 Chemical reactivity

Electrophilic addition to carbon-carbon multiple bonds is a very common and useful reaction type in organic chemistry, and the relative chemical reactivity of carbon-carbon double and triple bonds in proton addition reactions has been of particular interest (99; 100; 101). On one hand, alkynes are generally regarded as somewhat less reactive, provided that the reaction conditions are the same (100). On the other, structurally similar alkenes

and alkynes have about the same reactivity in acid-catalyzed hydration reactions and similar enthalpies of protonation in gas-phase proton additions (99; 102; 103; 104). With these different results in mind, the relative reactivity between alkenes and alkynes still remains to be clarified for this class of reactions.

Earlier studies have shown that carbon 1s ionization energies are closely related to activation energies in electrophilic addition reactions as well as enthalpies of protonation of alkenes, dienes and methylbenzenes (6; 105; 7; 8; 9). The C1s energies are linked to these reactivity parameters as follows. Positively charged species are formed in a carbon 1s ionization, similar to what we obtain in a protonation of an unsaturated hydrocarbon. To illustrate the resemblance between proton addition and core ionization, ethylene is used as an example in Scheme 1. Here, a proton addition is illustrated in **a** and C1s ionization in **b** where the core-ionized carbon is illustrated with an asterix.

Scheme 1:

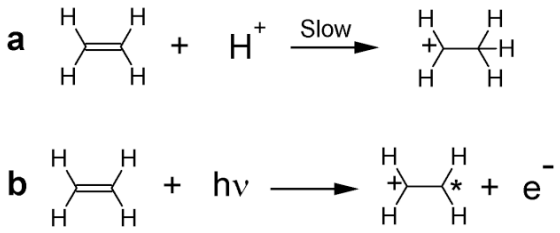

In both **a** and **b**, a positive charge is added to the carbon to the right. Because of charge redistribution, the left carbon obtains a positive charge in both **a** and **b**. The energies involved in these two processes are different, but it has been shown that the chemical effects that influence them are similar. In an electrophilic addition of a haloacid, however, a partial positive charge is added to one of the unsaturated carbon atoms. We consider protonation to represent a gas-phase model for the rate determining electrophilic attack in solution.

In paper IV, the chemical reactivity of twelve pairs of aliphatic and aromatic alkenes and alkynes has been explored from activation energies in electrophilic addition of HCl, enthalpies of protonation, and carbon 1s ionization energies. Furthermore, the pairs of alkenes and alkynes also facilitate a direct comparison of the reactivity of the two classes of compounds. All pairs are listed in Table 5.7, and among these compounds there are pairs that display the unsaturated bonds in terminal positions and those that possess the functional groups in internal positions.

Table 5.7: Alkenes and corresponding alkynes studied in paper IV. The table is adapted from paper IV.

ID[a]	Alkene	⟷	Alkyne
1	Ethene	⟷	Ethyne
2	Propene	⟷	Propyne
3	1-Butene	⟷	1-Butyne
4	Trans-2-butene	⟷	2-Butyne
5	1-Pentene	⟷	1-Pentyne
6	Trans-2-pentene	⟷	2-Pentyne
7	1-Hexene	⟷	1-Hexyne
8	Trans-2-hexene	⟷	2-Hexyne
9	Trans-3-hexene	⟷	3-Hexyne
10	1-Heptene	⟷	1-Heptyne
11	Styrene	⟷	Ethynylbenzene
12	4-Methylstyrene	⟷	4-Ethynyltoluene

[a]Identification number of each pair used to label the associated data entry in figures.

5.3.1 Activation energies and enthalpies of protonation

Activation energies in electrophilic addition of HCl have been calculated for the twelve pairs of alkenes and alkynes using the hybrid density functional B3LYP in combination with a modified TZP basis. These results are shown in Figure 5.14a, and the systematic lower activation energies of the alkenes suggest that the alkenes are more reactive towards HCl than are the alkynes.

Electrophilic addition reactions are expected to be closely related to protonation. Hence, enthalpies of protonation were computed for comparison between the alkenes and alkynes listed in Table 5.7 using the highly reliable G3 method (31). In Figure 5.14b, the alkyne enthalpies are plotted against the corresponding alkene enthalpies. With the exception of the ethane/ethyne point in the upper right corner of the figure, the alkene data are very similar to the alkyne data.

The reactivity data shown above have been compared with the C1s ionization energies of the double and triple bonded carbon atoms to explore the correlation between the different quantities. In Figure 5.15, enthalpies of protonation are plotted against C1s energies for both alkenes (top) and alkynes (bottom). The data points fall into two groups, one for the alkyl and one for the aryl substituents. The slopes for the alkyl substituents are close to 1, slightly larger for alkenes than for alkynes.

For the aryl substituents, the additional hydrogen introduced in the protonated species opens for an extension of the aromatic π system through a π-symmetry combination of s orbitals of the two hydrogens above and below the molecular π-system. No such orbital is available for core ionization,

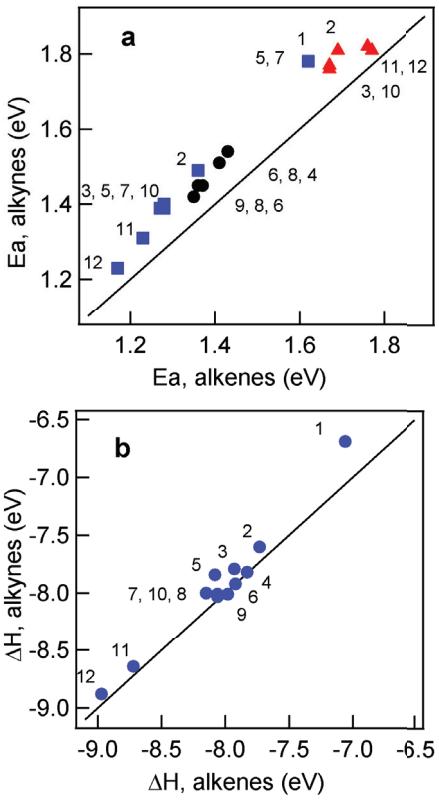

Figure 5.14: Computed alkyne activation energies (Ea) in HCl additions plotted against the alkene values (a), and computed enthalpies of protonation (ΔH) of the alkynes plotted against the corresponding alkene values (b). In the upper figure, the Markovnikov reactions are shown with blue squares, anti-Markovnikov additions with red triangles, and non-terminal with black circles. The solid lines have a slope of 1 and intercept of 0. See Table 5.7 for identification of compounds. The figure is adapted from paper IV.

making the effect of charge redistribution through resonance in the π system much larger for protonation than for core ionization. This difference has been noted earlier for processes taking place in the aromatic ring itself (7; 8; 9).

In Figure 5.16, activation energies for addition of HCl are plotted against C1s ionization energies, for alkenes (top) and alkynes (bottom) separately. Although there is a certain overall correlation, there is also considerable scatter. The data can be discussed in terms of three subsets: Markovnikov

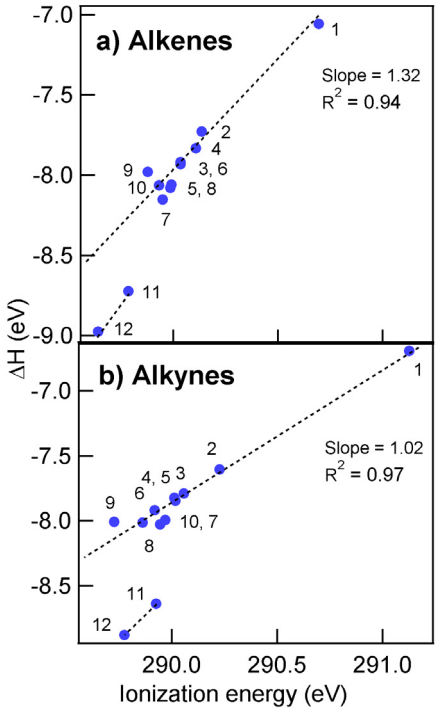

Figure 5.15: Computed enthalpies of protonation (ΔH) of alkenes (a) and alkynes (b) plotted against carbon 1s ionization energies. See Table 5.7 for identification of compounds. The figure is adapted from paper IV.

and anti-Markovnikov additions to terminal bonds, and addition to internal bonds.

First of all, we note that the Markovnikov data correlate reasonably well between the two quantities, with correlation coefficients (R^2) of 0.94 and 0.87 of the alkene and alkyne data set, respectively. The slope of the alkyne Markovnikov fit line (0.55) is larger than the corresponding alkene fit line (0.34), suggesting that the triple bond is more sensitive to substituent effects than is the double bond. However, C1s energies do not discriminate well among the anti-Markovnikov reactions. Similarily, core-level shifts do not look promising with respect to predicting the regiospecificity of HCl addition to internal double or triple bonds. As shown in paper IV, the deviations from the least-squares lines are due to differences in the geometric and electronic relaxation. Consequently, only terminal unsaturated bonds will be considered in the detailed analysis of the C1s shifts.

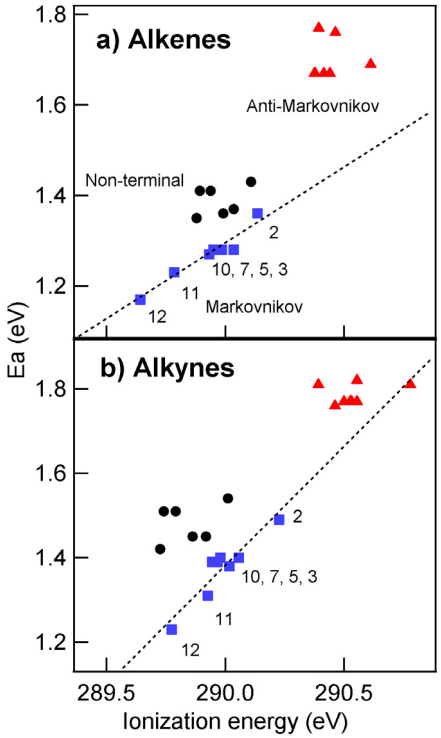

Figure 5.16: Computed activation energies (Ea) of HCl additions plotted against the carbon 1s ionization energies of alkenes (a) and alkynes (b). The red triangles represent the anti-Markovnikov values, the black circles the non-terminal values, the blue squares the Markovnikov values, and the dotted lines the Markovnikov least-squares fit lines. See Table 5.7 for identification of compounds. The figure is adapted from paper IV.

5.3.2 Carbon 1s shifts

In Figure 5.17, experimental C1s shifts relative to ethyne of the triple bonded carbon atoms of the alkynes presented in Table 5.7 are plotted against the corresponding alkene shifts, excluding the molecules with an internal double or triple bond. The figure shows that the alkenes have generally lower C1s ionization energies than the alkynes, supporting the view that the alkenes are more reactive than the alkynes in electrophilic addition reactions.

In order to explore this finding closer, the chemical shift, ΔI, was resolved into two contributions; ΔV, which one may think of as the electric potential in the core of the C1 carbon and is defined by the ground-state charge distribution, and ΔR, which is the effect of electronic and geometric

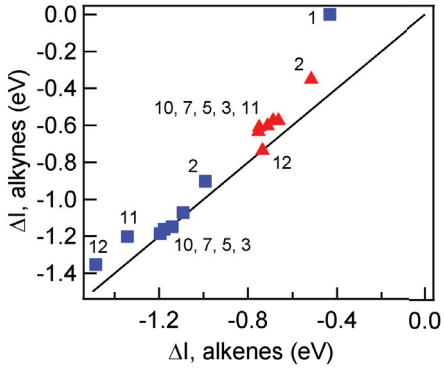

Figure 5.17: Carbon 1s shifts ΔI relative to ethyne of alkynes with terminal triple bonds plotted against the corresponding alkene shifts. The blue squares represent the C1 shifts, and the red triangles the C2 shifts. See Table 5.7 for identification of compounds. The figure is adapted from paper IV.

relaxation in the final state. These quantities are connected by the relationship $\Delta I = \Delta V - \Delta R$ (105; 106). As shown in paper IV, the ΔV and ΔR values are about 0.2 eV lower for the alkynes compared to the alkenes. Since ΔV and ΔR appear with opposite signs in ΔI, shifts in ionization energies between corresponding alkynes and alkenes are small.

5.3.3 Substituent effects

In paper IV, the effect of the substituent is investigated by considering the variation in activation energies and C1s ionization energies relative to ethene and ethyne. Shown in Figure 5.18, the energies are plotted as a function of alkyl and aryl substituents. To remove all effects that depend on location of the unsaturated bond in the carbon chain, only ionization and addition to the end carbon (C1) of the terminal unsaturated bonds are considered.

One feature of Figure 5.18 is that the shifts in activation energy (ΔEa) and ionization energy (ΔI) both decrease smoothly with increasing size of the alkyl substituent. The decrease is largest for the methyl group and then the effect levels off with increasing chain length. This behaviour may be understood from the combined effects of hyperconjugation and polarizability (65). Another apparent feature is the influence of the aryl groups which lowers both the shifts in ionization and activation energies more than the alkyl substituents. The results indicate that the major reason for this behaviour is due to the electronic relaxation in the final state. A third feature is that the effect of substituents is more pronounced for the triple bonds

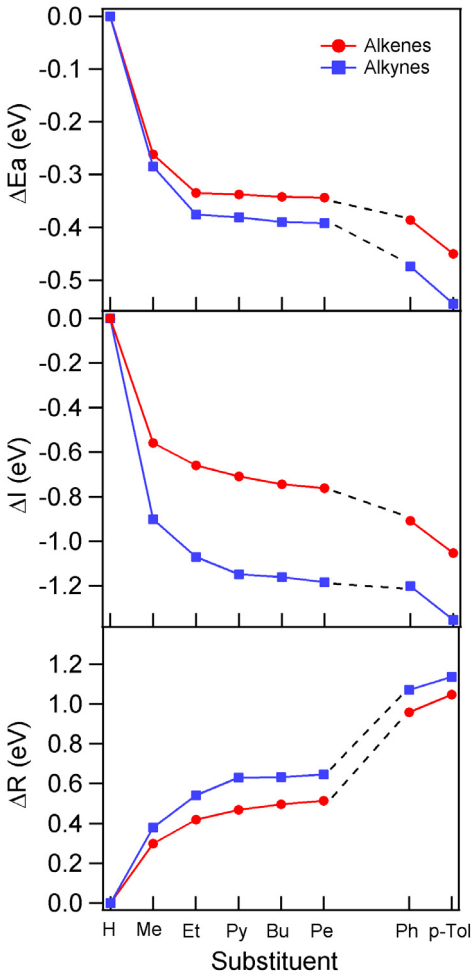

Figure 5.18: Activation energies, ΔEa (a), shifts in carbon 1s ionization energies, ΔI (b), and final-state relaxation energies, ΔR (c), plotted against the substituent. The alkene and alkyne values are plotted relative to that of ethene and ethyne, respectively, and show Markovnikov HCl addition to terminal alkenes and alkynes, and C1s ionization and relaxation at C1 of the same set of molecules. The figure is adapted from paper IV.

than for the double bonds.

5.3.4 Additivity of substituent effects

One way of summarizing substituent effects is to use linear additivity correlations. The model assumes that the total effect is equal to the sum of independent effects of the individual substituent (7; 8; 9). Using substituted alkynes as an example, we recognize that each alkyne has the formula $Y_\alpha C_\alpha C_\beta Y_\beta$, where Y_α and Y_β can be H, CH_3, a larger alkyl group, R, or an aryl group. If we ignore the aromatic groups, we can describe any alkyne by specifying, (α_{CH_3},α_R,β_{CH_3},β_R), where each α or β gives the number of substituents of the indicated type attached to $C_\alpha C_\beta$, respectively. Each α or β as well as the sums, $\alpha_{CH_3} + \alpha_R$ and $\beta_{CH_3} + \beta_R$, must be either zero or one. Ethyne, for example, is specified by (0,0,0,0). We consider C_α as the reactive carbon of interest. We can then make the following equation for the activation energies, Ea:

$$Ea = a\alpha_{CH_3} + b\alpha_R + c\beta_{CH_3} + d\beta_R + constant \tag{5.2}$$

The parameters a, b, c, and d have been determined from a least-squares fitting of all the activation energies of the alkynes. A similar expression has been written for the alkenes, and a constant term was included to allow for the difference between ethene and ethyne. For the activation energies, both the alkyne and alkene fits were found to be very good with correlation coefficients (R^2) larger than 0.99 and rms deviations of the points from the fits equal to or smaller than 10 meV. The parameters from the alkyne and alkene fits are summarized in Table 5.8.

Table 5.8: Additivity coefficients of the alkynes and alkenes summarized in 5.7, for the effect of methyl, alkyl or aryl substituents on the activation energies, in eV. Uncertainties in the last digit are shown in parentheses. For the aryl substituents the number of measurements is equal to the number of parameters. The table is adapted from paper IV.

Substituent	Position	Alkynes	Alkenes
CH_3	α	0.052 (6)	0.081 (4)
	β	-0.266 (6)	-0.259 (3)
R	α	0.013 (6)	0.059 (4)
	β	-0.364 (6)	-0.331 (4)
Ph	α	0.148	0.061
	β	-0.382	-0.449
Tol	α	0.158	0.051
	β	-0.442	-0.529
	Constant*	1.759 (6)	1.612 (4)

* Constant of the regression.

The offset of the alkyne data from the alkene data is seen in the difference

of 0.15 eV between the two intercepts (constants). In general, the parameters for the alkynes are very similar to those for the alkenes. For the replacement of a hydrogen atom on the carbon of interest by an alkyl group there is an increase in the activation energy. This is consistent with the higher electronegativity of the alkyl groups relative to hydrogen, which leads to more positive charge at this carbon, making it less receptive to attack by the hydrogen in HCl. A much larger effect of opposite sign is seen when the alkyl group is added in position β to the carbon of interest. Hyperconjugation leads to negative charge being transferred to C_α, with an accompanying lowering of the activation energy for Markovnikov addition. A similar trend is observed for the effect of aryl substituents on the activation energies. However, as can be seen in Table 5.8, the β effect is clearly larger for the aryl groups than it is for the alkyl groups.

Chapter 6

Conclusions

The main aim of this thesis has been to investigate the relationship between carbon 1s ionization energies and chemical reactivity in electrophilic addition of a range of alkenes and alkynes. However, a fraction of the molecules included in the study were found to possess two or more conformers. This made the analysis more complicated since the number of parameters is growing with the number of conformers. One way to reduce the number of parameters and secure reproducible and credible results from the C1s spectra, is to calculate chemical shifts in C1s ionization energy with high accuracy and use them as constraints in the spectral analysis. An investigation of the shift accuracy of different theoretical methods is therefore a prerequisite.

A database of 77 experimental carbon 1s ionization energies was prepared, covering linear and cyclic alkanes and alkenes, linear alkynes, and methyl- and fluoro-substituted benzenes. By comparing theoretical shifts with the corresponding experimental ones, an overview of the shift accuracy of a range of theoretical methods was prepared. Both *ab initio* and density functional theory (DFT) methods were included. Among the *ab initio* methods, the shifts calculated at the MP4SDQ/TZP and CCSD(T)/TZP levels of theory were found to have the highest accuracy with a root-mean-squared error (RMSE) of 29 and 32 meV, respectively. Among the selected DFT functionals, the BRx exchange functional in combination with the Perdew correlation functional P86 and the TZP basis was found to provide the shifts with highest accuracy with a RMSE of 55 meV. This accuracy is still inferior to the truly high-end *ab initio* methods. However, if an RMSE value of 50-60 meV is acceptable, DFT provides the opportunity to compute shifts of relatively large hydrocarbons.

Another factor that plays a role for the shift accuracy is the basis set. A rather unexpected result is observed when the cc-pVTZ basis is replaced with the TZP basis. For the most accurate DFT methods, the RMSE values decrease by about 40 meV, and the corresponding decrease among the high-end *ab initio* methods is about 20 meV. One possible reason for this result

is that the orbital exponent scaling factor used for the TZP ionized-carbon basis was optimized in the presence of the effective core potential (ECP).

With accurate theoretical predictions of chemical shifts available, it was possible to perform the analysis of complex spectra where two or more conformers provide unique atom-specific signal intensities to the spectrum. The investigations of the 1-pentyne conformers provided systematic methods for conformational analysis using theory-assisted XPS, and contributed to the ongoing debate in the literature about its conformational properties. The methodology was further developed for larger unsaturated hydrocarbons, where the complexity of the analysis increased correspondingly. In the cases where the molecule possesses more than two conformers, groups of conformers were identified and quantified rather than single conformers. The intramolecular 5-center CH/π interaction proved to play a crucial role. From similarities in shifts and vibrational profiles, it is appropriate to place all conformers in two separate groups depending on whether the conformer possesses the 5-center CH/π interaction or not. This implies that only two conformers are needed to describe the C1s photoelectron spectrum satisfactory; one for each group of conformers. However, this simplification also implies that we are not able to determine the population of all possible conformers a molecule may possess.

The relationship between the CH/π strength and experimental populations of conformers have also been investigated. In general, the *gauche* conformers of the alkynes are found to be more populated than the corresponding alkene *skew* conformers, taking into account the conformational degeneracies. CH/π stabilization energies computed at the M062X/TZP level of theory suggest that the CH/π interaction in the alkyne is stronger than in the corresponding alkene. The chemical shifts between *anti* and *gauche/skew* where the *gauche/skew* carbon atoms are oriented towards the π system, have also shown to be systematically larger for the alkynes than the corresponding alkenes. It is therefore a possibility that the CH/π interaction has an influence on the conformational populations and stabilities.

From the comprehensive analyses described above, the C1s ionization energies of twelve pairs of alkenes and corresponding alkynes were ready to be used to explore another property of unsaturated hydrocarbons; chemical reactivity in electrophilic addition reactions. The link between C1s ionization energies and chemical reactivity of such reactions is that in both cases a positive charge is added at one of the unsaturated carbons. A prerequisite for correlation between the different processes is that the energies involved are similarly influenced by the same molecular properties. In addition to the C1s ionization energies of the unsaturated carbons of the alkenes and alkynes, computed activation energies in electrophilic addition of HCl and enthalpies of protonation have been used as reactivity parameters. Here, we consider the protonation process as a highly ionic, limiting case of electrophilic addition. A comparison of the alkene and alkyne reactivity parame-

ters shows that the alkenes have systematically lower activation energies and hence higher reactivity than the alkynes, while the enthalpies of protonation are rather similar for the two classes of compounds. For the core-ionization energies, the trend is similar to the enthalpies of protonation provided that the unsaturated bond is located terminally.

A comparison of C1s energies and enthalpies of protonation shows that the two quantities are well correlated for the alkyl-substituted compounds with a slope of about 1, indicating that the energies involved are similarly influenced by the substituents for the two processes. The C1s energies correlate reasonably well with activation energies for both alkyl and aryl substituted molecules provided that the charge addition is restricted to Markovnikov addition to a terminal multiple bond. With slopes significantly lower than 1, the transition-state energy is less sensitive to substituent effects than is the ionization energy.

Triple bonds are found to have larger substituent effects than the double bond, shown from comparisons of alkenes and alkynes by using C1s energies and activation energies. This is in agreement with experimental data obtained from acid-catalyzed hydration reactions. A comparison of initial- and final-state effects exerted by the substituents shows that both the initial-state charge distribution and final-state charge redistribution for alkyl groups provide significant contributions to the shift. For the aryl substituents, however, the shift contribution from the final state is much larger than the initial-state contribution.

Chapter 7

Suggestions for further work

The conformational populations may be quantified either from the intensities of the conformational spectra, or the intensities of the vibrational profiles of the carbon atoms where significant differences in C1s ionization energy or vibrational lineshape are observed between the conformers. In conformational analysis, the number of degrees of freedom in the fitting models is large and the carbon peaks may be very close in C1s ionization energy. To secure credible and reproducible results, some of the analyses require that the intensity ratios between the different carbon atoms in each conformer are constrained to be the same (1:1) in the least-squares fitting routine. However, several examples both in the present work and other works (4; 107) show that there are exceptions to the 1:1 ratio, and that these deviations are mainly caused by scattering of the outgoing photoelectron. For instance, for 2-butyne explored in paper IV the C2 intensity is about 80% of the C1 intensity. A similar trend is seen for trans-2-butene and 3-hexyne. From these results, it is apparent that the 1:1 constraint is not the best solution to the problem of relative intensities. Conformational analyses and other analyses of complex spectra with 1:1 constraints may therefore be improved by applying methods that take into account the non-stiochiometric intensity ratios.

As mentioned in Section 3.11, very accurate calculations for methane, ethane, and ethylene show that the present level of theory exaggerates the contraction in C-H bonds that takes place during the ionization of sp^3 and sp^2 carbon atoms by 0.3 and 0.2 pm, respectively (61; 51; 45; 62). Furthermore, calculated harmonic frequencies are found to be slightly higher than the frequencies found experimentally (51; 63; 64). The C-H stretching modes on the core-ionized sp^3 carbon atoms were scaled by 0.95 (65), and the corresponding modes on the sp^2 carbons were scaled by 0.96 (45; 62). In the present work, the sp^3 corrections have also been used for the sp carbons. Therefore, it would be useful to perform accurate calculations to determine these corrections for the sp carbons.

Bibliography

[1] Hertz, H., *Ann. Physik* (1887) **31**, 983.

[2] Einstein, A., *Ann. Physik* (1905) **17**, 132.

[3] Siegbahn, K., *Phil. Trans. Roy. Soc. Lond. A.* (1970) **268**, 33–57.

[4] Travnikova, O., Børve, K. J., Patanen, M., Söderström, J., Miron, C., Sæthre, L. J., Mårtensson, N., and Svensson, S., *J. Electr. Spectrosc. and Relat. Phenom.* (2012) **185**, 191–197.

[5] J. Carwardine, G. Decker and R. Hettel, History of Synchrotron Radiation Sources, US Particle Accelerator School (USPAS), June 16-20, 2003.

[6] Sæthre, L. J., Thomas, T. D., and Svensson, S., *J. Chem. Soc., Perkin Trans. 2* (1997) p. 749.

[7] Carroll, T. X., Thomas, T. D., Bergersen, H., Børve, K. J., and Sæthre, L. J., *J. Org. Chem.* (2006) **71**, 1961–1968.

[8] Myrseth, V., Sæthre, L. J., Børve, K. J., and Thomas, T. D., *J. Org. Chem.* (2007) **72**, 5715–5723.

[9] Carroll, T. X., Thomas, T. D., Sæthre, L. J., and Børve, K. J., *J. Phys. Chem. A* (2009) **113**, 3481–3490.

[10] Abu-samha, M., Børve, K. J., Sæthre, L. J., and Thomas, T. D., *Phys. Rev. Lett.* (2005) **95**, 103002.

[11] Thomas, T. D., Sæthre, L. J., and Børve, K. J., *Phys. Chem. Chem. Phys.* (2007) **9**, 719–724.

[12] Http://www.maxlab.lu.se/beamlines/bli411/.

[13] Http://www-als.lbl.gov/als/techspecs/bl10.0.1.html.

[14] Attwood, D., *Soft X-rays and extreme ultraviolet radiation - Principles and applications*. Cambridge University Press, 1 edn. (2000).

[15] Hemmer, P. C., *Kvantemekanikk*. Tapir akademiske forlag, 2 edn. (2000).

[16] Koch, W. and Holthausen, M. C., *A Chemist's Guide to Density Functional Theory*. Wiley-VCH, 2 edn. (2001).

[17] Atkins, P. and Friedman, R., *Molecular Quantum Mechanics*. Oxford University Press, 4 edn. (2005).

[18] Pilar, F. L., *Elementary quantum chemistry*. Dover publications, inc., 2 edn. (2001).

[19] Dykstra, C. E., *Quantum chemistry and Molecular Spectroscopy*. Prentice-Hall (1992).

[20] Ellis, A., Feher, M., and Wright, T., *Electronic and Photoelectron Spectroscopy*. Cambridge University Press (2005).

[21] Hartree, D. R., *Proc. Camb. Phil. Soc.* (1928) **24**, 328.

[22] Fock, V. A., *Z. Phys.* (1970) **15**, 126.

[23] Pople, J. A., Binkley, J. S., and Seeger, R., *Int. J. Quantum Chem.* (1976) **Suppl. Y-10**, 1–19.

[24] Pople, J. A., Seeger, R., and Krishnan, R., *Int. J. Quantum Chem.* (1977) **Suppl. Y-11**, 149–163.

[25] Raghavachari, K. and Pople, J. A., *Int. J. Quantum Chem.* (1978) **14**, 91–100.

[26] Cizek, J., *Adv. Chem. Phys.* (1969) **14**, 35.

[27] Purvis, G. D. and Bartlett, R. J., *J. Chem. Phys.* (1982) **76**, 1910.

[28] Scuseria, G. E., Janssen, C. L., and Schaefer III, H. F., *J. Chem. Phys.* (1988) **89**, 7382.

[29] Scuseria, G. E. and Schaefer III, H. F., *J. Chem. Phys.* (1989) **90**, 3700.

[30] Lowe, J. P. and Peterson, K. A., *Quantum Chemistry*. Elsevier Academic Press, 3 edn. (2006).

[31] Curtiss, L. A., Raghavachari, K., Redfern, P. C., Rassolov, V., and Pople, J. A., *J. Chem. Phys.* (1998) **109**, 7764.

[32] Pople, J. A., Head-Gordon, M., Fox, D. J., Raghavachari, K., and Curtiss, L. A., *J. Chem. Phys.* (1989) **90**, 5622–5629.

[33] Curtiss, L. A., Jones, C., Trucks, G. W., Raghavachari, K., and Pople, J. A., *J. Chem. Phys.* (1990) **93**, 2537–2545.

[34] Curtiss, L. A., Raghavachari, K., Trucks, G. W., and Pople, J. A., *J. Chem. Phys.* (1991) **94**, 7221–7230.

[35] Fermi, E., *Rend. Accad. Lincei* (1927) **6**, 602.

[36] Thomas, L. H., *Proc. Camb. Phil. Soc.* (1927) **23**, 542.

[37] Hohenberg, P. and Kohn, W., *Phys. Rev. B* (1964) **136**, 864.

[38] Kohn, W. and Sham, L., *Phys. Rev. A* (1965) **140**, 1133.

[39] Becke, A. D., *J. Chem. Phys.* (1993) **98**, 5648–5652.

[40] Attwood, D., *A chemist's guide to density functional theory*. Wiley-VCH, 2 edn. (2001).

[41] Stevens, W. J., Basch, H., and Krauss, M., *J. Chem. Phys.* (1984) **81**, 6026.

[42] DALTON, a molecular electronic structure program, Release 2.0 (2005), see http://www.kjemi.uio.no/software/dalton/dalton.html.

[43] Børve, K. J. and Thomas, T. D., *J. Electron Spectrosc. Relat. Phenom.* (2000) **107**, 155–161.

[44] Børve, K. J., Sæthre, L. J., Thomas, T. D., Carroll, T. X., Berrah, N., Bozek, J. D., and Kukk, E., *Phys. Rev. A* (2000) **63**, 012506.

[45] Myrseth, V., Børve, K. J., Wiesner, K., Bässler, M., Svensson, S., and Sæthre, L. J., *Phys. Chem. Chem. Phys.* (2002) **4**, 5937.

[46] Siggel, M. R. F., Field, C., Sæthre, L. J., Børve, K. J., and Thomas, T. D., *J. Chem. Phys.* (1996) **105**, 9035.

[47] Bozek, J., Carroll, T. X., Hahne, J., Sæthre, L. J., True, J., and Thomas, T. D., *Phys. Rev. A* (1998) **57**, 157.

[48] Hahne, J. A., Carroll, T. X., and Thomas, T. D., *Phys. Rev. A* (1998) **57**, 4971.

[49] Thomas, T. D., Sæthre, L. J., Sørensen, S. L., and Svensson, S., *J. Chem. Phys.* (1998) **109**, 1041.

[50] Kivimäki, A., Kempgens, B., Maier, K., Köppe, H. M., Piancastelli, M. N., Neeb, M., and Bradshaw, A. M., *Phys. Rev. Lett.* (1997) **79**, 998.

[51] Karlsen, T., Sæthre, L. J., Børve, K. J., Berrah, N., Kukk, E., Bozek, J. D., Carroll, T. X., and Thomas, T. D., *J. Phys. Chem. A* (2001) **105**, 7700.

[52] Kempgens, B., Köppel, H., Kivimäki, A., Neeb, M., Cederbaum, L. S., and Bradshaw, A. M., *Phys. Rev. Lett.* (1997) **79**, 3617.

[53] Frisch, M. J., et al., Gaussian 03, Revision C.02. Gaussian, Inc., Wallingford, CT, 2004.

[54] Frisch, M. J., et al., Gaussian 09 Revision A.1. Gaussian Inc. Wallingford CT 2009.

[55] Dunning, T. H., Jr, *J. Chem. Phys.* (1971) **55**, 716.

[56] Raghavachari, K., Binkley, J. S., Seeger, R., and Pople, J. A., *J. Chem. Phys.* (1980) **72**, 650.

[57] McLean, A. D. and Chandler, G. S., *J. Chem. Phys.* (1980) **72**, 5639.

[58] G2FC program, K. J. Børve, Department of Chemistry, University of Bergen, Norway, 1999.

[59] A2FC program, K. J. Børve, Department of Chemistry, University of Bergen, Norway, 2012.

[60] Hedberg, L. and Mills, I. M., *J. Mol. Spectrosc.* (2000) **203**, 82–95.

[61] Karlsen, T. and Børve, K. J., *J. Chem. Phys.* (2000) **112**, 7986.

[62] K. J. Børve, unpublished material.

[63] Carroll, T. X., Berrah, N., Bozek, J. D., Hahne, J., Kukk, E., Sæthre, L. J., and Thomas, T. D., *Phys. Rev. A* (1999) **59**, 3386.

[64] Shimanouchi, T., Mallard, W. G., Linstrom, P. J., and Eds., *NIST Chemistry WebBook, NIST Standard Reference Database (http://webbook.nist.gov), National Institute of Standards and Technology: Gaithersburg, MD* (2000) **69**.

[65] Karlsen, T., Børve, K. J., Sæthre, L. J., Wiesner, K., Bässler, M., and Svensson, S., *J. Am. Chem. Soc.* (2002) **124**, 7866–7873.

[66] Igor Pro 6.22A; WaveMetrics, Inc., Lake Oswego, OR, USA.

[67] Spectral Analysis by Curve Fitting Macro Package SPANCF. Available from: http://www.physics.utu.fi/en/research/material_science /Fitting.html.

[68] van der Straten, P., Morgenstern, R., and Niehaus, A., *Z. Phys. D.* (1988) **8**, 35.

[69] Enkvist, C., Lunell, S., and Svensson, S., *Chem. Phys.* (1997) **214**, 123–130.

[70] Sorensen, S. L., Børve, K. J., Feifel, R., de Fanis, A., and Ueda, K., *J. Phys. Chem. B* (2008) **41**, 095101.

[71] Steiner, T., *Angew. Chem. Int. Ed.* (2002) **41**, 48–76.

[72] Nishio, M., Hirota, M., and Umezawa, Y., *The CH/π interaction. Evidence, nature, and consequences.*. Wiley-VCH (1998, p. 51).

[73] Takagi, T., Tanaka, A., Matsuo, S., H., M., Tani, M., Fujiwara, H., and Sasaki, Y., *J. Chem. Soc., Perkin Trans. 2* (1987) .

[74] Takahashi, O., Kohno, Y., and Nishio, M., *Chem. Rev.* (2010) **110**, 6049–6076.

[75] Bell, S., Drew, B. R., Guirgis, G. A., and Durig, J. R., *J. Mol. Struct.* (2000) **553**, 199–219.

[76] Bell, S., Zhu, X., Guirgis, G. A., and Durig, J. R., *J. Mol. Struct.* (2002) **616**, 135–158.

[77] Bell, S., Guirgis, G. A., Li, Y., and Durig, J. R., *J. Phys. Chem. A* (1997) **101**, 5987–5996.

[78] Durig, J. R., Drew, B. R., Koomer, A., and Bell, S., *Phys. Chem. Chem. Phys.* (2001) **3**, 766–775.

[79] Fraser, G. T., Xu, L.-H., Suenram, R. D., and Lugez, C. L., *J. Chem. Phys.* (2000) **112**, 6209.

[80] Purvis, G. D. and Bartlett, R. J., *J. Phys. Chem. A* (2000) **104**, 1141.

[81] Woller, P. B. and Garbisch Jr., E. W., *J. Org. Chem.* (1972) **37**, 4281–4285.

[82] Wu, F., Chen, X., Shan, X., Tian, S. X., Li, Z., and Xu, K., *J. Phys. Chem. A* (2008) **112**, 4360–4366.

[83] Trætteberg, M., Bakken, P., and Hopf, H., *J. Mol. Struct.* (1999) **509**, 213–220.

[84] Rizzo, T. R., Park, Y. D., Peteanu, L. A., and Levy, D. H., *J. Chem. Phys.* (1986) **84**, 2534.

[85] Page, R. H., Shen, Y. R., and Lee, Y. T., *J. Chem. Phys.* (1988) **88**, 4621.

[86] Lipert, R. J. and Colson, S. D., *J. Phys. Chem.* (1989) **93**, 3894.

[87] Robertson, E. G. and Simons, J. P., *Phys. Chem. Chem. Phys.* (2001) **3**, 1–18.

[88] Shubert, V. A. and Zwier, T. S., *J. Phys. Chem. A* (2007) **111(51)**, 13283–13286.

[89] Blanco, S., Sanz, M. E., Lopez, J. C., and Alonso, J. L., *PNAS* (2007) **104(51)**, 20183–20188.

[90] The number of nondegenerate conformers can be calculated from the formula $1/2(3^{N_b}+1)$ where N_b is the number of bonds the different nondegenerate conformers can be obtained by rotation. The sum of both degenerate and nondegenerate conformers can be calculated from 3^{N_b}.

[91] Durig, J. R. and Drew, B. R., *J. Mol. Struct.* (2001) **560**, 247–259.

[92] Damiani, D. and Mirri, A. M., *Chem. Phys. Lett.* (1971) **10(4)**, 351–354.

[93] Wodarczyk, F. J. and Wilson, E. B., *J. Chem. Phys.* (1972) **56**, 166–176.

[94] At the time when the 1-pentyne paper was published, chemical shifts had only been computed at the HF, MP2, B3LYP, and CCSD(T) levels of theory in combination with the cc-pVTZ basis set. The results with the Dunning TZP basis set as well as the DFT results were produced after submitting the 1-pentyne paper for publication.

[95] Crowder, G. A., *J. Mol. Struct.* (1988) **172**, 151–156.

[96] Atticks, K. A., Bohn, R. K., and Michels, H. H., *Int. J. Quantum Chem.* (2001) **85**, 514–519.

[97] Utzat, K., Bohn, R. K., and Michels, H. H., *J. Mol. Struct.* (2007) **841**, 22–27.

[98] Boys, S. F. and Bernardi, F., *Mol. Phys.* (1970) **19**, 553.

[99] Melloni, G., Modena, G., and Tonellato, U., *Acc. Chem. Res.* (1981) **14**, 227.

[100] Carey, F. A. and Sundberg, R., *Advanced Organic Chemistry: Structure and mechanisms*. Springer, 5 edn. (2007).

[101] Mascavage, L. M., Zhang-Plasket, F., Sonnet, P. E., and Dalton, D. R., *Tetrahedron* (2008) **64**, 9357–9367.

[102] Yates, K., Schmid, G. H., Regulski, T. W., Garratt, D. G., Leung, H.-W., and McDonald, R., *J. Am. Chem. Soc.* (1973) **95:1**, 160–165.

[103] Modena, G., Rivetti, F., and Tonellato, U., *J. Org. Chem.* (1978) **43**, 1521–1526.

[104] Marcuzzi, F., Melloni, G., and Modena, G., *J. Org. Chem.* (1979) **44**, 3022–3028.

[105] Thomas, T. D., Sæthre, L. J., Børve, K. J., Gundersen, M., and Kukk, E., *J. Phys. Chem. A* (2005) **109**, 5085.

[106] Sæthre, L. J., Berrah, N., Bozek, J. D., Børve, K. J., Carroll, T. X., Kukk, E., Gard, G. L., Winter, R., and Thomas, T. D., *J. Am. Chem. Soc.* (2001) **123**, 10729.

[107] Söderström, J., et al., *Phys. Rev. Lett.* (2012) **108**, 193005.